

A population study of type II bursts in the Rapid Burster

T. Bagnoli,^{1,2★} J. J. M. in 't Zand,¹ C. R. D'Angelo³ and D. K. Galloway^{4†}

¹*SRON Netherlands Institute for Space Research, Sorbonnelaan 2, NL-3584 CA Utrecht, the Netherlands*

²*Astronomical Institute 'Anton Pannekoek', University of Amsterdam, Postbus 94249, NL-1090 GE Amsterdam, the Netherlands*

³*Leiden Observatory, Leiden University, Postbus 9513, NL-2300 RA Leiden, the Netherlands*

⁴*Monash Centre for Astrophysics (MoCA), Monash University, Clayton, VIC 3800, Australia*

Accepted 2015 February 12. Received 2015 February 10; in original form 2014 December 19

ABSTRACT

Type II bursts are thought to arise from instabilities in the accretion flow on to a neutron star in an X-ray binary. Despite having been known for almost 40 years, no model can yet satisfactorily account for all their properties. To shed light on the nature of this phenomenon and provide a reference for future theoretical work, we study the entire sample of *Rossi X-ray Timing Explorer* data of type II bursts from the Rapid Burster (MXB 1730–335). We find that type II bursts are Eddington-limited in flux, that a larger amount of energy goes in the bursts than in the persistent emission, that type II bursts can be as short as 0.130 s, and that the distribution of recurrence times drops abruptly below 15–18 s. We highlight the complicated feedback between type II bursts and the NS surface thermonuclear explosions known as type I bursts, and between type II bursts and the persistent emission. We review a number of models for type II bursts. While no model can reproduce all the observed burst properties and explain the source uniqueness, models involving a gating role for the magnetic field come closest to matching the properties of our sample. The uniqueness of the source may be explained by a special combination of magnetic field strength, stellar spin period and alignment between the magnetic field and the spin axis.

Key words: stars: neutron – X-rays: binaries – X-rays: bursts – X-rays: individual: MXB 1730–335.

1 INTRODUCTION

X-ray bursts observed in accreting neutron stars (NS) in low-mass X-ray binaries (LMXBs) come in two types, sometimes similar in appearance (~ 1 min time-scales, 10^{38} erg s^{-1} peak luminosities) but thought to be due to very different mechanisms, because of the large difference (by factors $\sim 10^2$) in average power.

Type I bursts arise from the heating and cooling of the NS photosphere after a thermonuclear shell flash of accreted material (see reviews by Lewin, van Paradijs & Taam 1993; Strohmayer & Bildsten 2006; Galloway et al. 2008). This is consistent with thermal spectra of varying temperature and roughly constant emitting area. Despite some remaining open questions (e.g. Cornelisse et al. 2003; Suleimanov, Poutanen & Werner 2011; Watts 2012), a general understanding of the physics underlying type I bursts has been reached, also thanks to the wide range of circumstances in which they occur (type of LMXB, accretion rates, etc.) provided in particular by the relatively large amount of bursters (over a hundred).

Type II bursts remain largely a puzzle. Soon after their discovery, Hoffman, Marshall & Lewin (1978) showed that their short recurrence times rule out the possibility that they are powered by nuclear burning, ascribing the source instead to gravitational potential energy. Little more is understood about their origin, also because they are only confidently detected in two sources: the Rapid Burster (MXB 1730–335, hereafter RB), a recurring transient which is the object of this study and which also exhibits type I bursts, and the Bursting Pulsar (BP), a slowly rotating (2 Hz) accretion-powered pulsar (Kouveliotou et al. 1996).

One of the first properties of type II bursts discovered in the RB is the relaxation-oscillator behaviour: the fluence in a type II burst is proportional to the waiting time to the next burst (Lewin et al. 1976). This is not observed in the BP (Kouveliotou et al. 1996). The relaxation-oscillator behaviour seems to point to the presence of a mass storage from which matter can be released and then replenished at a constant rate, so that the amount of depleted material determines the time to refill the buffer (Lewin et al. 1993). The accretion disc is the most obvious candidate for this buffer and all proposed models involve one (e.g. Walker 1992; Spruit & Taam 1993). The various time-scales at different positions in the disc can help to explain the range of observed type II burst time-scales, while a key role in acting as a gating mechanism might be played by a

*E-mail: t.bagnoli@sron.nl

†Also at School of Physics, and Astronomy, Monash University, Clayton, VIC 3800, Australia.

magnetic field (e.g. recent simulations by Kulkarni & Romanova 2008; D’Angelo & Spruit 2010, 2012; Romanova et al. 2012).

Notwithstanding that models involving some role for the NS magnetic field seem promising, the strength of the magnetic field is unfortunately not known in the RB due to the lack of pulsations. For the BP, estimates of the surface strength of the dipolar component of the magnetic field B put it in the range $(2\text{--}6) \times 10^{10}$ G (Degenaar et al. 2014). While this is larger than in typical NS LMXBs (Lewin et al. 1993), it is not unique among bursters (estimates put the magnetic field of the NS in IGR J17480–2446 at $10^9\text{--}10^{10}$ G; e.g. Cavecchi et al. 2011). Therefore, at least another parameter besides the magnetic field strength (e.g. the stellar spin, or the inclination of B with respect to the stellar spin axis) must determine the type II burst occurrence.

Bagnoli et al. (2013, hereafter B13) have shown that thermonuclear (type I) X-ray bursts in the RB occur over an unusually large range of accretion luminosities, from about 45 per cent of the Eddington luminosity L_{Edd} (assuming it is located in the globular cluster Liller 1 at a distance of 7.9 ± 0.9 kpc; Valenti, Ferraro & Origlia 2010) down to almost quiescence (Masetti et al. 2000). However, while the type I bursts span the entire range of luminosities, type II bursts only appear below a critical luminosity of about 10 per cent L_{Edd} (Guerriero et al. 1999, B13). Hence, there are a type-I-only phase and a mixed phase.

The type-I-only state is a soft state because the persistent emission spectrum is dominated by a disc blackbody component, and it spans the range 10–45 per cent of L_{Edd} . This is almost unique among type I burst sources: all other bursters show nearly no type I bursts above $L \sim 0.1L_{\text{Edd}}$ (Cornelisse et al. 2003), except for the slow (11 Hz) pulsar IGR J17480–2446 (Linares et al. 2012). The abundance of type I bursts in the RB above this threshold prompted B13 to propose that it is a slow rotator too, and to speculate that this might actually be one of the necessary ingredients for producing type II bursts.

As the RB exits the soft state, the first type II bursts appear. These first type II bursts are the most energetic, long and infrequent. A brief (typically a few days) intermediate state exists in which these are accompanied by double-peaked type I bursts and a quasi-periodic oscillation (QPO) at 0.25 Hz (Bagnoli et al. 2014, hereafter B14). The unusual shape of the type I bursts found in this short-lived intermediate outburst phase seems to be due to a temporary obscuration of the NS surface during the burst decay, producing the double peaks. The ensuing type II bursts, the obscuration phenomenon and the occurrence of a QPO are probably related to the change in the accretion geometry that is widely thought to take place between the soft and the hard state (e.g. review by Done, Gierliński & Kubota 2007, and references therein).

Having studied the soft and intermediate states in our aforementioned papers, we now complete our study of the entire *Rossi X-ray Timing Explorer* (*RXTE*, 1995–2012) RB data base by focusing on the type-II-burst-dominated hard state, so called because of the power-law component that dominates the persistent emission spectrum. We aim at constructing a population study of type II bursts to compare it with the predictions of the few available theoretical models, and as a future reference. In Section 2, we introduce the data set, and in Section 3 we illustrate our methodology. In Section 4, we present the type II burst properties and their relationship with the persistent emission and the type I bursts, taking advantage of the unprecedented detail provided by the *RXTE* data. We summarize our findings, some of which were previously unknown, in Section 5, and discuss their physical implications in Section 6. Finally, in Section 7 we review proposed theoretical models, checking their predictions against the properties of our sample.

2 OBSERVATIONS

2.1 The general sample and burst identification

This study is about measurements with the Proportional Counter Array (PCA) onboard *RXTE*. It consists of five co-aligned proportional counter units (PCUs) that combine to a total photon collecting area of 8000 cm² over a 2 to 60 keV bandpass (Jahoda et al. 2006).

Nearly all *RXTE* observations of the RB (exposure time 2.4 Ms) were carried out in one of three configurations. For 553 ks, the PCA was directly pointed at the source. These observations are contaminated by the presence of the persistently bright 4U 1728-34 at an angular distance of 0°:56. For 612 ks, the pointing was offset by just this amount, thus avoiding the contamination at the expense of roughly half the effective area. Finally, for 1.3 Ms the PCA was pointed at 4U 1728-34, serendipitously encompassing the RB. We have investigated all of the 2.4 Ms of data.

We extracted a light curve from the ‘STANDARD-1’ data for all the observations containing the RB in the field of view (FOV). These data have 0.125 s time resolution and no photon energy resolution. The telescope orientation was determined with the *FTOOL* *PCACLRSP*, and deemed stable if the jitter was below 20 arcsec.

We performed a visual inspection of all the light curves. For the details of source (RB versus 4U 1728-34) and burst (type I versus type II) identification, we refer the reader to Appendix A. In total, we identified 123 type I and 8458 type II bursts from the RB.

2.2 Type II bursting modes

As already mentioned, type II bursts are only emitted by the RB at persistent luminosities below 10 per cent of the Eddington limit (B13; Guerriero et al. 1999), when the RB is in the hard state (B14). Actually, the RB almost never reaches higher luminosities during outbursts after 1999 (Masetti 2002; B14).

Three modes of type II bursting behaviour follow one another in a smooth transition, differing in light curves, energetics and bursting patterns (Marshall et al. 1979; Guerriero et al. 1999). To illustrate the evolution of the type II burst behaviour, we plot the light curve from *RXTE* data of the outburst in 2006 June–July (Fig. 1).

The first type II bursts are hundreds of seconds long, often with flat peaks and have the longest recurrence times (sometimes longer than a few ks observation). The persistent emission drops right before and after them. These are the so-called mode-0 type II bursts (Fig. 1, top-left inset). We identified a record long mode 0 burst with a duration of at least 1100 s. It is visible in Fig. 1 as the long plateau on June 26.

At lower persistent fluxes, the large bursts are increasingly preceded by sequences of 8 to 40 short bursts. After the final longer burst, a longer gap is measured, during which the persistent emission rises to a level higher than that of the intraburst emission, in a ‘hump’ shape. This bursting pattern is called mode 1 (Fig. 1, top-right inset).

As the outburst decays further, the sequences of mode-1 type II bursts become increasingly long, the final bursts less energetic and the humps shorter and less pronounced. Eventually, all bursts have similar energetics and durations: this is the so-called mode 2 (Fig. 1, bottom-middle inset). Finally, even these bursts become increasingly sparse, as the source moves to quiescence (Fig. 1, bottom-right inset).

We caution that the sequence ‘no type II bursts → mode 0 → mode 1 → mode 2’ is only a *general* trend. For instance, the flat peak in Fig. 1 starting on June 27 is not a very long mode-0 type II

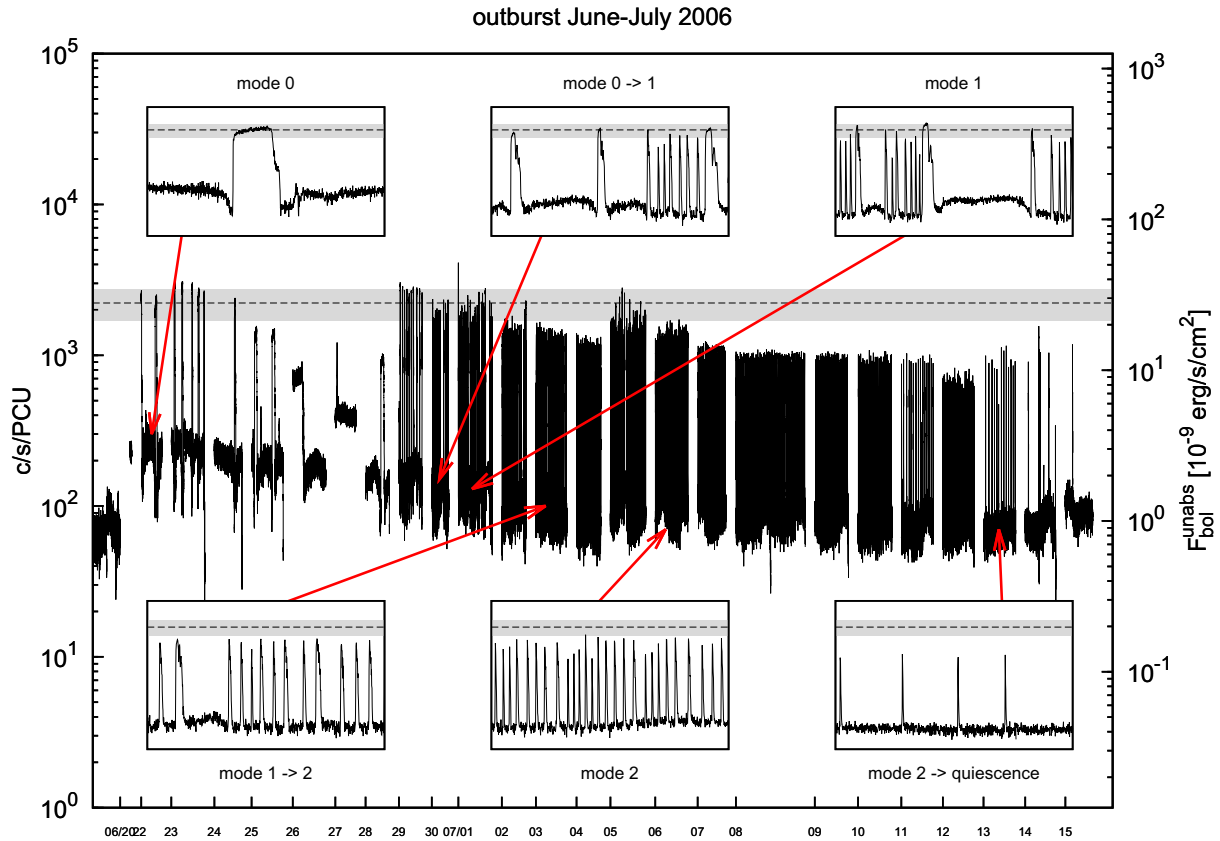


Figure 1. Sandwiched light curve of the observations of the outburst starting on 2006 June 20, for the complete PCA bandpass at 1 s resolution. Each consecutive data stretch is typically about 3000 s long. Data gaps mark jumps in time when there were no observations. Photon count rate per PCU is on the left y-axis, unabsorbed bolometric flux on the right y-axis. The horizontal dashed line indicates the Eddington luminosity, with the grey-shaded area indicating the uncertainties on the distance and the spectral fit (see Section 3.1). Count rates are not background subtracted in this plot, but are corrected for the number of active PCUs and the collimator response. (throughout the rest of the paper, the background counts have been subtracted). 4U 1728-34 was never in the FOV. The non-zero count rates before the onset of the outburst are therefore due to the instrumental background and the galactic ridge emission (see fig. 2 in Valinia & Marshall 1998). The insets show the varying (following in time left to right, top to bottom) type II bursting modes during the outburst decay. Each inset shows 1 ks of data, plotted logarithmically between 50 and 5000 $\text{c s}^{-1}\text{PCU}^{-1}$. This outburst shows the prototypical sequence mode 0 \rightarrow mode 1 \rightarrow mode 2 in bursting behaviour. The soft state, however, does not appear at the beginning of the outburst, hence preceding the type II bursting phase as in most cases, but it is briefly entered by the RB around June 27, giving rise to the long flat peak around that date. Note that the shorter plateau visible on June 26 is actually the longest type II burst in our sample, at about 1100 s (see Section 4.2).

burst, but an actual switch of the source to the soft state, during which a type I burst can be seen, but no type II bursts. Two observations were taken the day before and the day after showing long mode-0 type II bursts, meaning that the soft state lasted briefly.

Also, the RB can sometimes be seen switching back and forth between modes. The switch is sudden rather than gradual (as shown in Fig. 2, already noted by Lewin et al. 1993), although the RB can be seen to transit back and forth between modes for a few ks. It is clear from the picture that the minima before and after a mode-0 burst are not ‘dips’: rather, the humps in between are what is peculiar and are a feature common to all very energetic type II bursts, independent of bursting mode.

The sampling along an outburst is often patchy, meaning that it is not easy to establish an average duration for each mode. The outburst in Fig. 1 is probably the best sampled one. It features the longest mode-0 phase in the entire data set, lasting ≈ 8.7 d, albeit including a brief return into the soft state. The longest uninterrupted mode-0 bursting phase occurred in an earlier outburst, and lasted ≈ 6.5 d. Mode-1 bursts are visible in Fig. 1 for ≈ 2.1 d. In a later outburst, they were observed to last for twice that time, ≈ 5.2 d.

Finally, mode-2 bursts were continuously observed for up to 24 d, the longest stretch in the data set.

2.3 The type II burst sample

Our search routine found 8458 type II bursts in the entire data set (see Section 2.1). The results are summarized in Table 1. We determined the instrumental and cosmic diffuse background with the `FTOOL_PCABACKEST`. No bursts were analysed that are outside so-called good time intervals, are affected by data gaps or overlapping with type I bursts (from either the RB or 4U 1728-34), or are in ObsIDs for which the collimator response was not constant because of a slew. This left us with 7601 bursts.¹ Of these, 3662 type II bursts are present in 389 ks of direct pointings, while 3183 were observed during 341 ks of offset pointings, and 756 during 92 ks of 4U 1728-34 observations.

¹ A table including all the burst properties for the entire sample is available online.

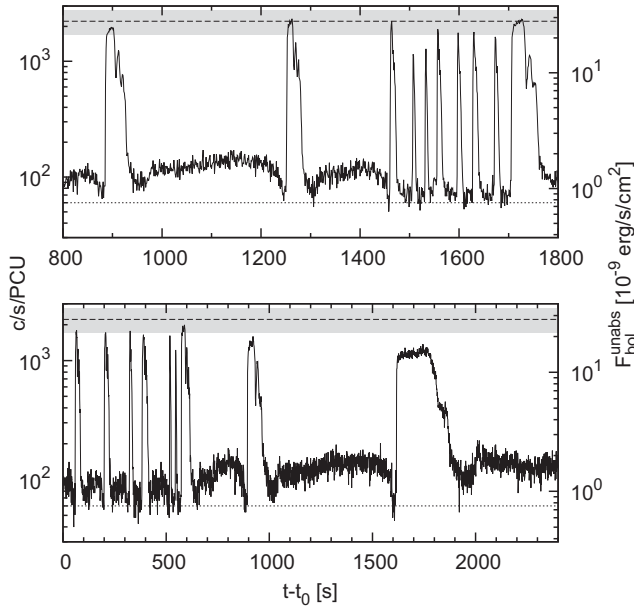


Figure 2. Examples of mode switching, $0 \rightarrow 1$ (top panel) and $1 \rightarrow 0$ (bottom panel). Time axis with respect to the start of the ObsID. The y-axes are as in Fig. 1. The horizontal dashed line indicates the Eddington luminosity, with the grey-shaded area indicating the uncertainties on the distance and the spectral fit (see Section 3.1). The dotted line shows $F_{\text{pers}}^{\text{min}} = 60 \text{ c s}^{-1} \text{ PCU}^{-1}$. The quiescent level between quick bursts is the same as the dip level before and after mode-0 bursts. The RB therefore does not ‘dip’ but rather shows humps of enhanced emission after long type II bursts.

Table 1. The sample of analysed^(a) type II bursts.

Bursting mode ^(b)	Number of bursts per aimpoint ^(c)		Total
	RB	offset 1728-34	
0	78	24	104
1	964	895	2522
2	2620	2260	4971
Unclear	0	4	4
All	3662	3183	7601

Notes. ^(a)About 800 bursts identified by our routine were not analysed, see Section 2.1.

^(b)For a description of the bursting patterns, see Section 2.2.

^(c)The different orientations of the telescope in the data and their effect on FOV contamination and effective area are discussed in Section 2.1.

In total, the RB was stably in mode 0 during the entirety of an ObsID for 114 ks, in mode 1 for 170 ks and in mode 2 for 492 ks. In 51 ks of data, the behaviour was intermediate between two consecutive modes, switching often back and forth during the transition. We found 104 mode-0 bursts, 2522 mode-1 bursts and 4971 mode-2 bursts. For four bursts taking place during very short observations (a few hundred seconds), we could not clearly assign a mode.

Furthermore, during 210 ks of data, the RB was at such a high luminosity that only type I bursts were observed (B13). Finally, no RB bursts of either type were found in ObsIDs totalling 1.4 Ms (mostly in observations with the instrument pointed at 4U 1728-34), when the RB was in quiescence.

3 METHODOLOGY

3.1 Counts as proxy for energy

We adopted the photon counts as a proxy for the energy flux, rather than fitting time-resolved spectra. This approach offers an obvious advantage in speed of the data reduction. Furthermore, the intraburst persistent emission would often be too short and weak to constrain the spectrum well. Finally, the flux variations, which can be very large during type II bursts, are largely achronatic; it is mostly the normalization factor and not the intrinsic spectral shape that is changing. This is shown in Appendix B, where we perform time-resolved spectroscopy on a representative selection of the type II bursts. We obtained the best fits with a Comptonization model (COMPTT in XSPEC Titarchuk 1994). The conversion factor between PCA counts and 3–25 keV fluence is $1.02 \times 10^{-11} \text{ erg cm}^{-2}$ per c/PCU. The uncertainty induced by the spectral shape is 10 per cent (full range, not 1σ). The bolometric correction would be 1.24 ± 0.07 for the COMPTT model.

For a ‘canonical’ NS (mass $M = 1.4 M_{\odot}$), the Eddington luminosity L_{Edd} is $2.1 \times 10^{38} \text{ erg s}^{-1}$. This assumes isotropic emission, no gravitational redshift and an accreted H fraction $X = 0.7$ because the RB type I bursts show long (100 s) tails that are typical of burning of H-rich material. For a distance of $(7.9 \pm 0.9) \text{ kpc}$, this yields a flux $F_{\text{Edd}} = (2.8 \pm 0.3) \times 10^{-8} \text{ erg cm}^{-2} \text{ s}^{-1}$. Given the above conversion to the bolometric flux, and propagating the relative errors on the spectral shape, bolometric correction and distance, the Eddington luminosity in the RB corresponds to $F_{\text{Edd}}^{\text{PCA}} = (2200 \pm 500) \text{ c s}^{-1} \text{ PCU}^{-1}$.

3.2 Extracting the sample properties

For each type II burst, we calculated from the STANDARD-1 light curve the start time and duration t_{dur} at 0.125 s accuracy by seeking backward and forward in time for the first two consecutive time bins where the count rate was below the persistent emission level. This way, we also determined Δt^{prev} and Δt^{next} , the recurrence times with respect to the previous and the next burst, respectively, as the difference between the start times. Because the burst duration can be a significant fraction of the duty cycle for type II bursts (unlike for most type I bursts), the actual non-bursting time can be significantly shorter than the recurrence times so defined.

We defined two different measurements of the intraburst persistent flux. First, we calculated the actual intraburst fluence E_{pers} and divided that by the intraburst time, providing the average persistent flux (F_{pers}). In a vast majority of cases, the instantaneous flux was stable during the interval, and deviated little from the average.

As mentioned in Section 2.2, the persistent emission however tends to rise after very energetic bursts (the mode-0 and end-of-sequence mode-1 bursts), reaching a minimum immediately before and after those bursts. Therefore, for the purpose of measuring the net burst emission properties, we also calculated the average count rate $F_{\text{pers}}^{\text{min}}$ in the 10 s before a burst (or less, when Δt^{prev} is shorter). This assumes that, during the burst, the persistent emission will be stable at the minimum level reached right before it.

We made this choice for two reasons. First, this assumption has long been part of the standard approach to burst analysis (e.g. Galloway et al. 2008). Secondly, the reappearance of the persistent emission at roughly the same flux after the energetic bursts (see e.g. Fig. 2) supports our choice.

We subtracted $F_{\text{pers}}^{\text{min}}$ from the observed count rates to calculate the net burst emission properties. We defined the peak flux F_{peak}

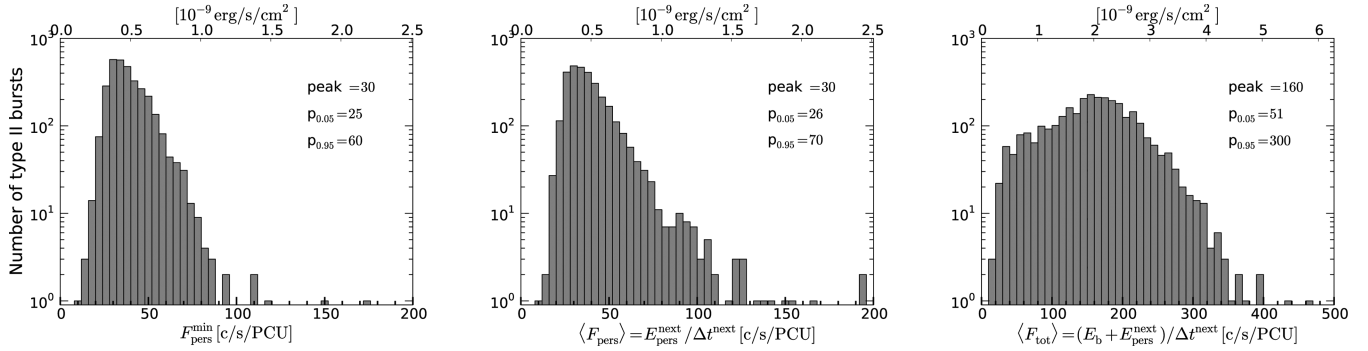


Figure 3. Histograms of all persistent flux parameters (see Section 4.1): the persistent count rate immediately before a burst $F_{\text{pers}}^{\text{min}}$, the average persistent count rate after a burst (F_{pers}) and the total average flux (including the burst) (F_{tot}). The peak of the distribution, 5th and 95th percentiles are indicated for each parameter. Only bursts that were not contaminated by 4U 1728-34 have been included (see Section 2.1).

and the total burst fluence E_b as the maximum net count rate and the integrated burst net counts during this interval.

The ratio of E_{pers} to E_b is the parameter α , which is key to distinguishing between type I and II bursts, because the ratio of the fluence liberated in the persistent emission to that the burst diagnoses whether the latter can be explained by thermonuclear burning of the accreted material or not. For reasons that will become clearer in Section 4.2, we defined two values of α for each burst, employing E_{pers} *before* and *after* the burst: thus, we retrieved a backward-defined α^{prev} and a forward-defined α^{next} . The previous is the parameter that is normally employed in studies of type I bursts, but as we will see, the latter shows a more significant relationship for type II bursts.

We subtracted the instrumental background counts (calculated and interpolated from STANDARD-2 data in 16 s resolution) from all quantities, and then normalized them by the number of active PCUs and the correction given by the telescope orientation (see Section 2.1). Clearly, all quantities related to the persistent emission have to be considered upper limits (lower for α) when the FOV is contaminated by 4U 1728-34. We did not include these in our analysis.

4 RESULTS

4.1 The persistent emission

First, we look at the properties of the persistent emission when the RB is emitting type II bursts, whenever not contaminated by 4U 1728-34 (see Section 2.1). We plot the various properties in Fig. 3, with the peak of the distribution (the highest bin) and the 5 and 95 percentiles indicated.

The average persistent emission count rate before a burst $F_{\text{pers}}^{\text{min}}$ is limited to a narrow range of values, with 90 per cent of the distribution between 25 and 60 $\text{c s}^{-1}\text{PCU}^{-1}$, or $\simeq (0.01\text{--}0.025)F_{\text{Edd}}$. Therefore, no bursts are observed on top of a null net persistent emission. The largest observed value is 110 $\text{c s}^{-1}\text{PCU}^{-1}$, corresponding to $\simeq 0.05F_{\text{Edd}}$ (note that at times when there are no type II bursts, the persistent flux can be as high as $\simeq 0.45F_{\text{Edd}}$).

As explained in Section 3.2, this is only a lower limit on the actual intraburst emission. However, short mode-1 and mode-2 bursts make up the majority of our sample, so that the following histogram, of the average persistent count rates after a burst (F_{pers}), shows a very similar distribution, with a slightly longer tail. The minimum

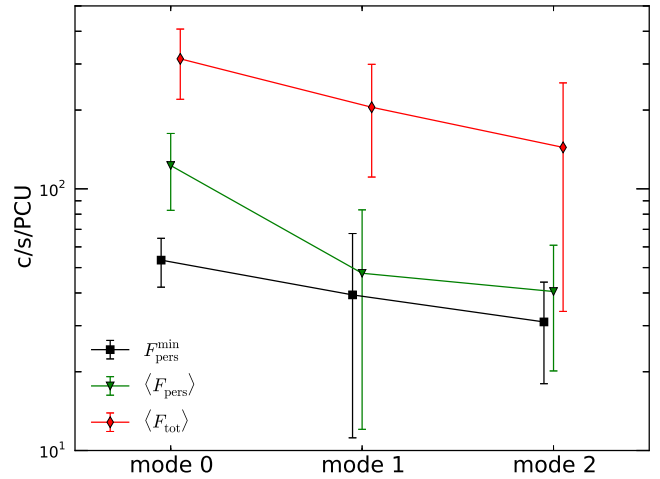


Figure 4. The average values of $F_{\text{pers}}^{\text{min}}$, $\langle F_{\text{pers}} \rangle$ and $\langle F_{\text{tot}} \rangle$ during mode-0, -1 and -2 type bursts (see Section 4.1). The error bar indicates the standard deviation in each sample.

values are similar to those of $F_{\text{pers}}^{\text{min}}$ because the persistent emission never dips between bursts, but only right before and after them. The maximum of the distribution is larger with respect to $F_{\text{pers}}^{\text{min}}$, with all but 10 bursts showing $\langle F_{\text{pers}} \rangle < 200 \text{ c s}^{-1}\text{PCU}^{-1} \simeq 0.09F_{\text{Edd}}$.

Since both the persistent emission and the type II bursts probably originate from the release of gravitational energy (although possibly through different channels), the total average flux in the interval between two bursts Δt , including both the burst and persistent emission, is also a potential proxy for the actual mass accretion rate of the RB during the hard state (under the assumption that the radiative efficiency is similar for the persistent emission and the type II bursts). We call this flux $\langle F_{\text{tot}} \rangle$, and plot it in the following histogram in Fig. 3. The bursts seem to increase the accretion flux by a factor of ~ 4 , up to an upper limit of 400 $\text{c s}^{-1}\text{PCU}^{-1}$, or $\simeq 0.17F_{\text{Edd}}$. Therefore, an average 75 per cent of the accretion goes through bursts.

All three measurements show a monotonically decreasing trend from mode 0 to 1 to 2, as plotted in Fig. 4. However, the dispersion within each sample is similar or larger than the difference in values between modes. We obtained the same result trying to reproduce the same figure for the outburst plotted in Fig. 1 alone. It seems therefore that the persistent emission variations only marginally trace the changing type II burst behaviour.

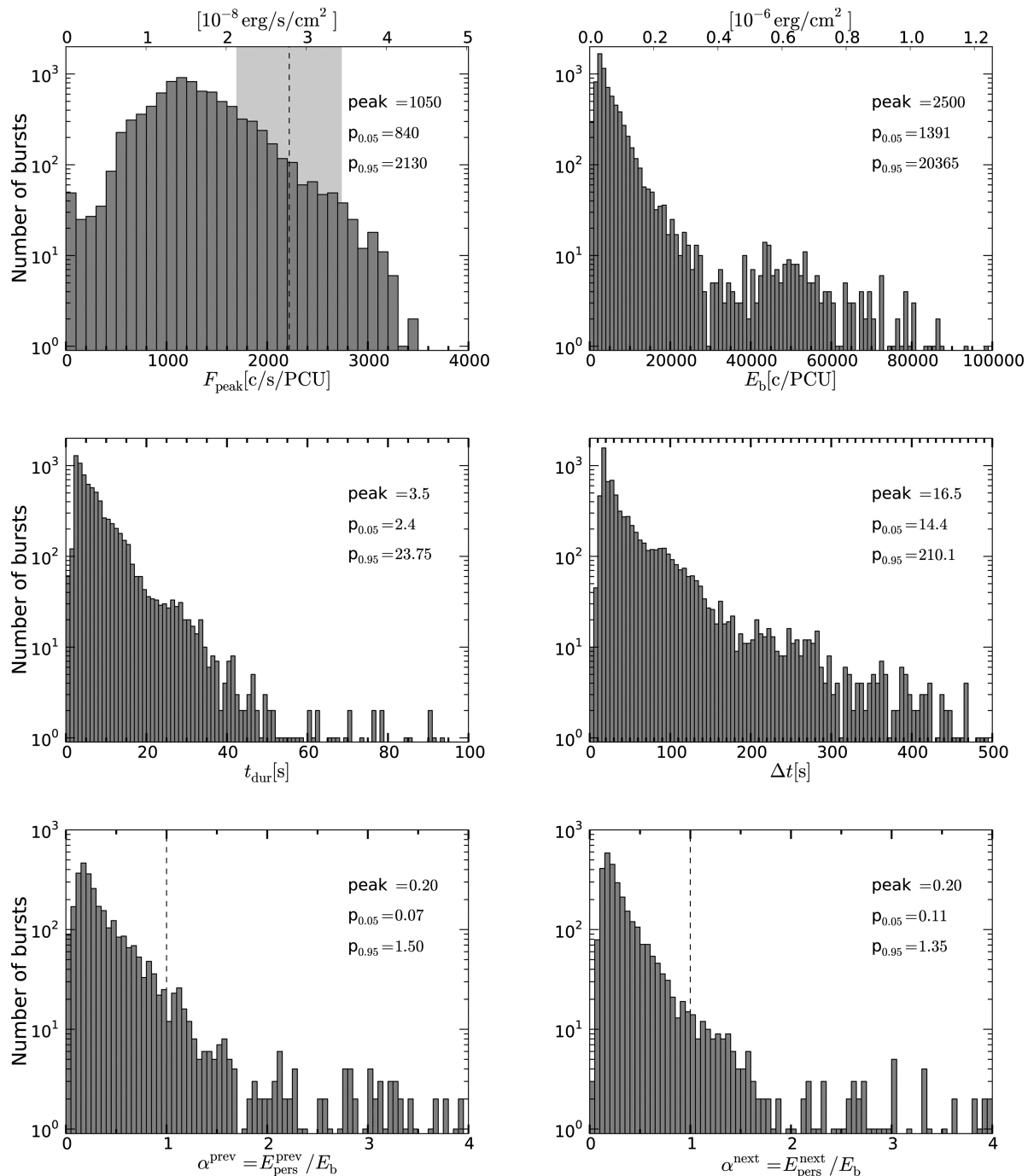


Figure 5. Histograms of all burst parameters. The peak of the distribution, 5th and 95th percentiles are indicated for each parameter. The dashed line in the left-top plot is the flux corresponding to the Eddington luminosity for $M = 1.4 M_{\odot}$, $X = 0.73$. The grey area reflects the uncertainty in the spectral fit (see Appendix B). The shortest observed $\Delta t = 2$ s, $t_{\text{dur}} = 0.125$ s. The dashed line in the α plots divides the regions where the burst fluence exceeds that of the persistent emission and vice versa. α values have only been computed for observations that were not contaminated by 4U 1728-34 (see Section 2.1).

4.2 The type II bursts

For all 7601 analysed type II bursts, we study their energetics (peak flux F_{peak} and fluence E_b) and time-scales (duration t_{dur} and recurrence time Δt). Furthermore, we investigate their relationships to the persistent emission properties for the 3183 bursts observed when 4U 1728-34 is outside the FOV. In Fig. 5, we have plotted histograms of the burst properties, again annotated with the peak of the distribution (the highest bin) and the 5 and 95 percentiles.

4.2.1 Burst properties

Starting with the distribution of peak fluxes of type II bursts, the peak is at about half the Eddington luminosity, or $1100 \text{ c s}^{-1} \text{ PCU}^{-1}$. Overall, the distribution is relatively narrow, with 90 per cent of the bursts peaking in the range $(1.1\text{--}2.7) \times 10^8 \text{ erg cm}^{-2} \text{ s}^{-1}$. The distribution seems compatible with being Eddington limited. Only 1 per cent of the bursts are above the upper limit on L_{Edd} given by the uncertainty over the distance and the

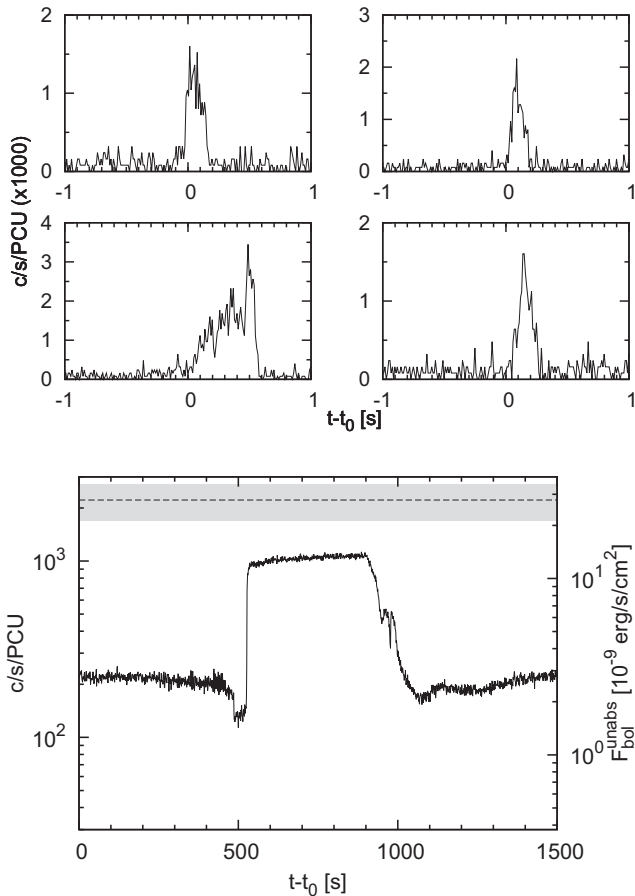


Figure 6. Top: examples of some of the shortest bursts in the sample from the 10 ms resolution light curve of ObsID 92026-01-08-05 (2006 July 20). Left y-axis is as in Fig. 1. The bursts take place during an otherwise ordinary sequence of mode-2 type II bursts. Bottom: for comparison, the longest entirely observed burst in the sample, at 533.125 s, from ObsID 40058-02-03-01S (1999 April 20). The y-axes are as in Fig. 1. The flat top is substantially below the Eddington limit, indicated by the horizontal dashed line, with the grey-shaded area indicating the uncertainties on the distance and the spectral fit (see Section 3.1). A longer burst ($\gtrsim 1100$ s, see Fig. 1 and Section 4.2) was only partially observed.

spectral fit (see Section 3.1; this limit is actually more clear in Figs 7–9).

A larger dynamic range of values is observed for the burst fluences, which span about three orders of magnitude, making for a fairly large distribution. The majority of bursts are in mode 1 or 2, so it is not surprising that many show a relatively small fluence. These bursts radiate typically between 10^{-8} and several 10^{-7} erg cm $^{-2}$. The more energetic mode-0 bursts show minimum fluences of several 10^{-7} erg cm $^{-2}$. 42 mode-0 bursts show $E_b > 10^{-6}$ erg cm $^{-2}$, peaking at $E_b^{\max} = 5.8 \times 10^{-6}$ erg cm $^{-2}$.

The durations of type II bursts can vary by four orders of magnitude, although 90 per cent of them last between 2.4 and 23.75 s. The shortest bursts actually challenge the time resolution of STANDARD-1 data of 0.125 s, and need to be resolved in event-mode data (Fig. 6, top). The shortest burst in our sample only lasted 130 ms. We found 61 bursts with sub-second durations, all during mode-2 bursting phases towards the end of an outburst, 46 of them in ObsID 92026-01-08-05 alone.

These very short bursts do not show peak fluxes smaller than the rest of the sample. Their fluences are however some of the smallest

observed, liberating on average $\sim 5 \times 10^{-9}$ erg cm $^{-2}$. Their light curves tend to show very fast rises and equally fast decays, although they can have shapes that are unseen in the rest of the sample (such as the burst in the bottom-left panel of Fig. 6, which has a gradual rise and a sudden decay).

The longest burst observed in its entirety lasts 533 s (Fig. 6, bottom). The record holder is however a burst lasting at least 1100 s, the rise of which was not caught in the observation. Only 26 bursts recorded durations longer than 100 s, all but two being mode-0 bursts.

The recurrence times are mostly below 200 s (again, with the exception of the mode-0 bursts), the shortest and the longest (without data gaps) Δt being 2 and 1656 s, respectively. Overall, the distribution is extremely asymmetric. This is logical, since the shorter the recurrence time, the more bursts will be observed. The peak of the distribution is however well above zero, at $\Delta t = 15$ –18 s. Below this bin, the distribution drops abruptly. Concerning mode-0 bursts, their recurrence times (excluding lower limits) range between 105 and 1562 s.

For the 3183 bursts that were in observations uncontaminated by 4U 1728-34, we compared the fluence released in the burst to that in the persistent emission. We calculated the α^{prev} and α^{next} values, respectively, by dividing the integrated fluence in the interval prior and after the burst by the total burst fluence E_b . The former is the parameter that is employed when dealing with type I bursts, since thermonuclear bursts are due to the burning of material *after* this has been accreted. Fig. 5 shows that the values of α^{prev} for type II bursts peak at 0.20, meaning more energy is released in the bursts than in the persistent emission. They are incompatible with the values expected from thermonuclear burning ($\simeq 40$ at least, for H-rich fuel; Lewin et al. 1993, and the minimum measured $\alpha \simeq 10$; Keek et al. 2010).

Even at the lowest persistent fluxes, when the RB approaches quiescence and the type II burst frequency drops, (see bottom-right inset of Fig. 1), $\alpha^{\text{prev}} < 10$. The only type II bursts with larger α^{prev} values are those with sub-s durations, which can have $\alpha^{\text{prev}} \sim 20$ –200, but are much shorter than type I bursts.

The type II bursts are thought to draw from the same energy reservoir as the persistent emission. Also, their occurrence and properties seems to affect the persistent emission that follows, rather than to depend on the persistent emission that precedes them (see below). Because of this, we also plot the integrated ratio of the fluence *following* a burst to the integrated burst fluence, α^{next} . The two distributions are similar, although that of α^{next} is narrower and does not approach values as small as the other one. The final large bursts in mode 1 sequences tend to have short Δt_{prev} (the time interval to the previous burst), and long Δt_{next} . Hence, their α^{prev} are smaller than their α^{next} .

4.2.2 Correlations

Having described the burst properties individually, we turn our attention to the relationships between them. As we show in Fig. 7, some burst properties show trivial correlations. The burst fluence E_b correlates with both the peak flux F_{peak} (Spearman rank-order correlation coefficient $\rho = 0.57$) and, more strongly, with the burst duration t_{dur} ($\rho = 0.90$), with the mode-0 bursts having the largest E_b and longest t_{dur} . In the lower left corner of the upper plot are the bursts for which almost the entire fluence is emitted in a short interval around the burst peak (in the lower plot these bursts are mostly shorter than 10 s). At the opposite end of the top plot, the

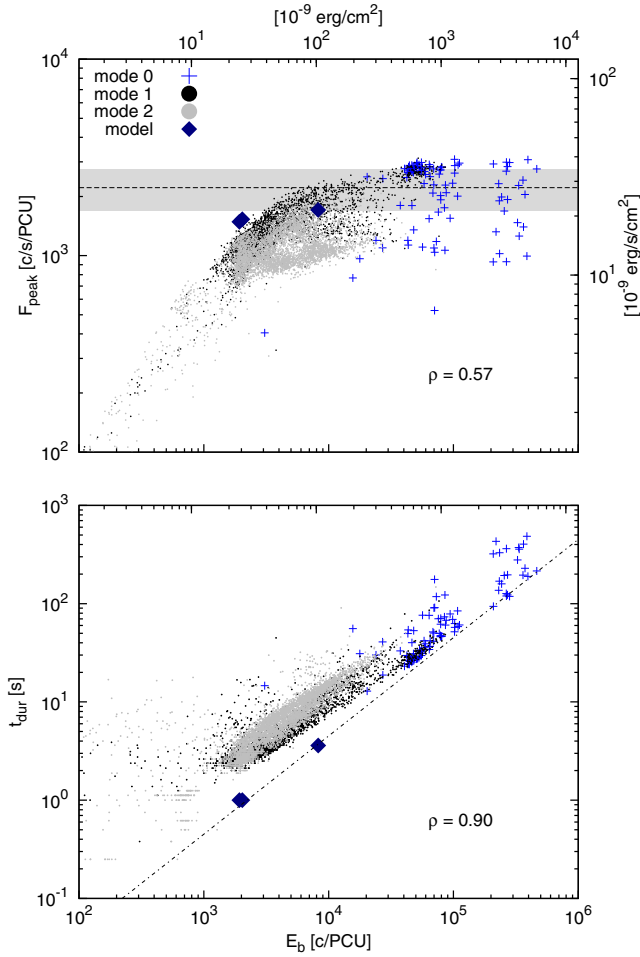


Figure 7. Peak flux F_{peak} and burst duration t_{dur} as a function of the burst fluence E_b (see Section 4.2). Count rates and energies are as in Fig. 1. The horizontal dashed line indicates the Eddington luminosity, with the grey-shaded area indicating the uncertainties on the distance and the spectral fit (see Section 3.1). The correlation (given by the Spearman correlation factor ρ) is strong in both cases, although it saturates in the upper plot at the flux corresponding to the Eddington luminosity. The dash-dotted line in the bottom plot indicates the duration of an Eddington-limited burst of a given fluence. The red diamonds are the values predicted by three the models in Fig. 15, with two of them nearly overlapping (see Section 7.1).

correlation between F_{peak} and E_b saturates once the peak flux reaches the Eddington limit. There seems to be no correlation between peak flux and duration (not plotted).

It is also interesting to see how these quantities, which determine the burst energetics, depend on the bursting rate at a given moment. Fig. 8 shows the type II burst peak flux, fluence and duration as a function of the recurrence time to the next burst Δt^{next} . On top, one can see that F_{peak} is roughly independent of the waiting time ($\rho = 0.04$). A correlation instead appears in the middle panel, which plots E_b against Δt^{next} ($\rho = 0.71$): this is the well-known relaxation-oscillator behaviour of the RB, according to which the more energetic a burst, the longer it takes for the next one to occur. This is the reason why we chose to introduce the parameter α^{next} . However, a look at the bottom plot in Fig. 8 reveals that Δt^{next} correlates more tightly with t_{dur} ($\rho = 0.87$) than with E_b . This implies that the duration of a type II burst, rather than the energy it releases, determine the time it takes for the next type II burst to occur. A least-squares fit yielded $t_{\text{rec}} \propto (\Delta t^{\text{next}})^{0.76 \pm 0.01}$. There is,

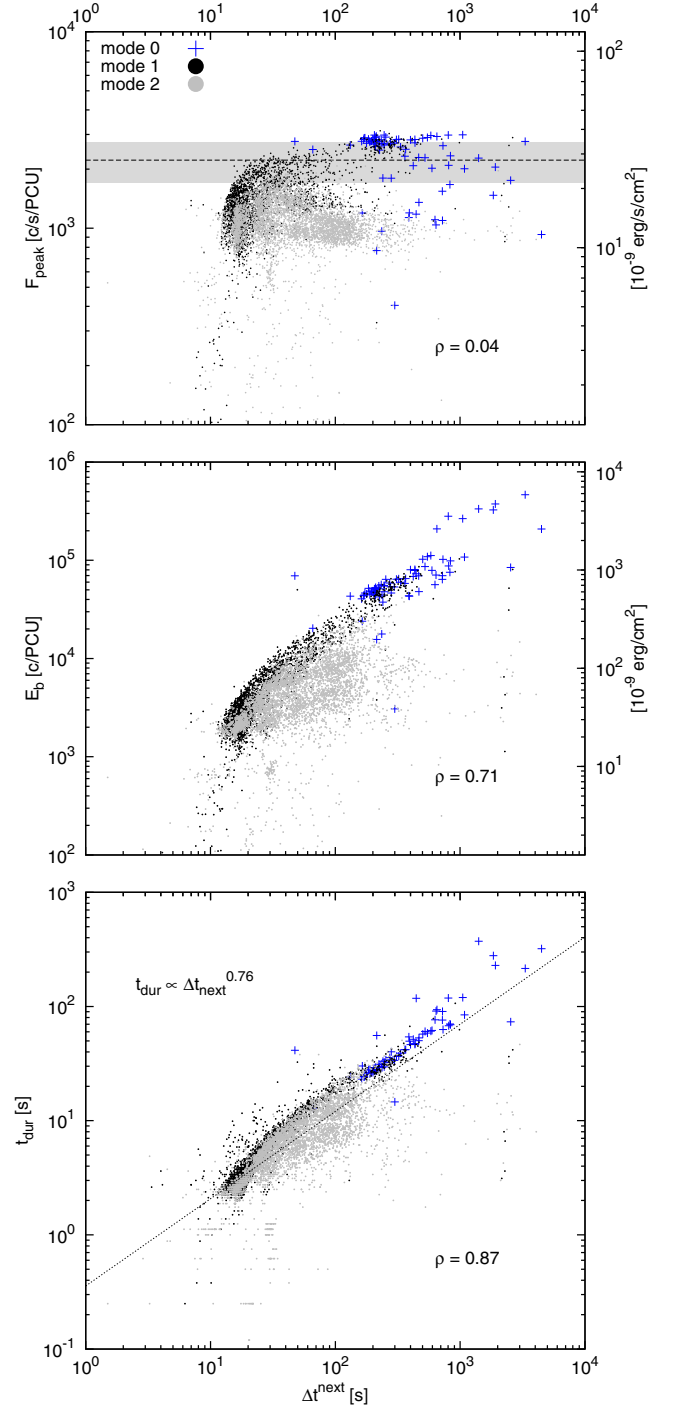


Figure 8. Burst peak flux F_{peak} , fluence E_b , duration t_{dur} as a function of the waiting time Δt to the next burst (see Section 4.2). Count rates and energies are as in Fig. 1. The horizontal dashed line indicates the Eddington luminosity, with the grey-shaded area indicating the uncertainties on the distance and the spectral fit (see Section 3.1). The middle and bottom plot show the relaxation oscillator behaviour of the type II bursts; the burst recurrence time seems to more accurately predicted by the duration of the previous burst than its fluence. The least-squares fit to the data in the bottom plot is also shown with a dotted line (see Section 4.2).

however, a large spread in the data, especially for the mode-1 and mode-2 bursts.

As we explained in Section 2.2 different patterns of type II bursts follow each other during the outburst decay, while on average the

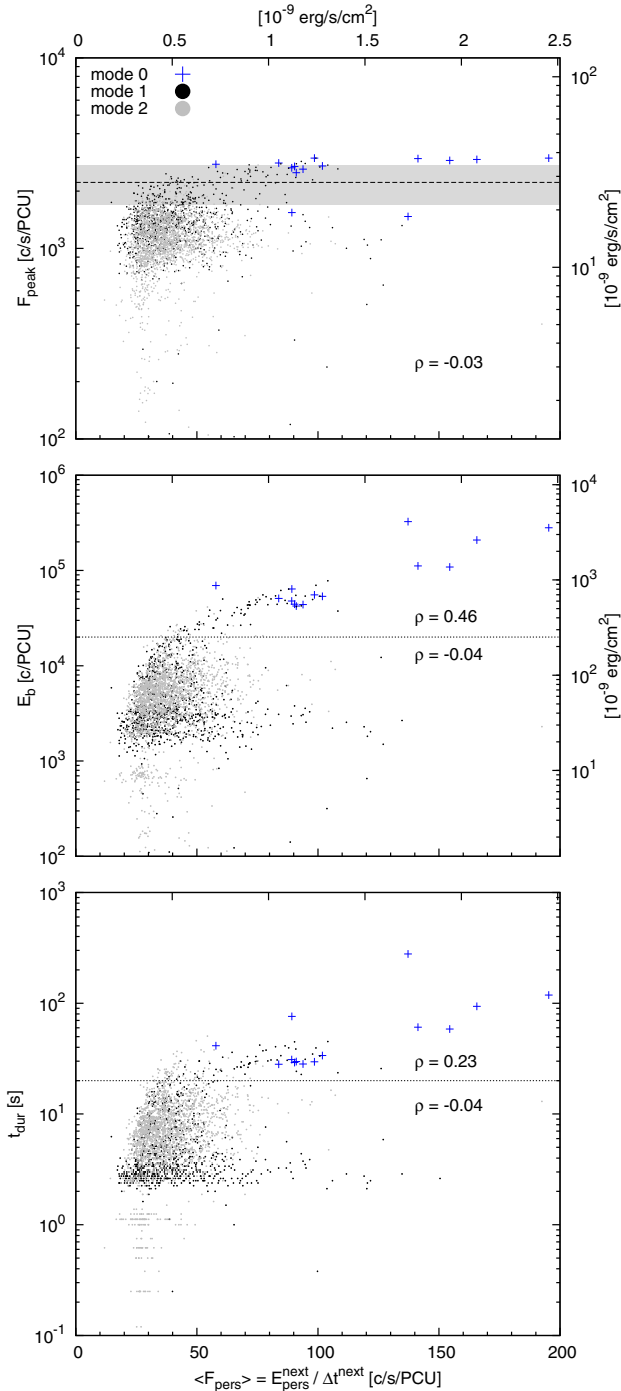


Figure 9. Same burst properties as in Fig. 8, here plotted against the average persistent flux $\langle F_{\text{pers}} \rangle$ (see Section 4.2 for definition). Only bursts observations that were not contaminated by 4U 1728-34 are plotted (see Section 2.1). Count rates and energies are as in Fig. 1. The horizontal dashed line indicates the Eddington luminosity, with the grey-shaded area indicating the uncertainties on the distance and the spectral fit (see Section 3.1). No overall correlation is visible in the data, although it might hold for the longest, most energetic bursts (see Section 4.2).

persistent flux decreases. We therefore wish to assess whether the burst properties show any dependence on the strength of the persistent emission. Fig. 9 shows the burst peak flux, fluence and duration plotted against the average persistent flux $\langle F_{\text{pers}} \rangle$. It is immediately evident that all correlations are weaker than with respect to Δt^{next} .

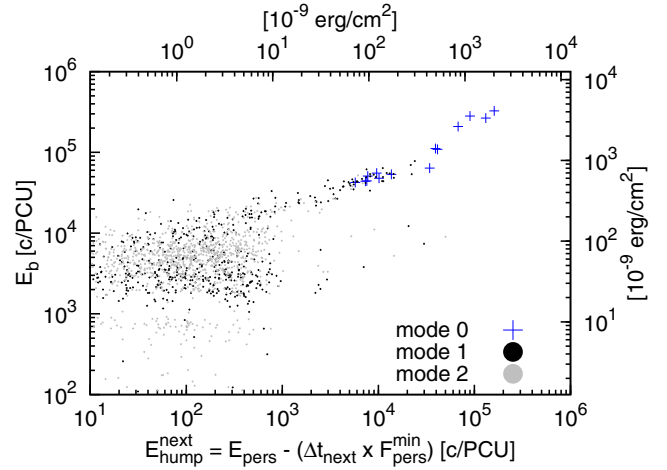


Figure 10. The burst fluence E_b against the ‘net’ (i.e. above $F_{\text{pers}}^{\text{min}}$) hump fluence E_{hump} (see Section 4.2). Count rates and energies are as in Fig. 1. Above a critical $E_b \sim 2 \times 10^4$ c/PCU, a correlation appears. Both the brightest mode-1 bursts and all mode-0 bursts can be above this threshold.

As in the previous case, F_{peak} shows no evident relation to the persistent emission properties ($\rho = -0.03$). In the middle and bottom panels, where we plot E_b and t_{dur} against $\langle F_{\text{pers}} \rangle$, no monotonic trends can be seen. Instead, two distinct behaviours appear. While for bursts that liberate little fluence ($E_b \lesssim 2 \times 10^4$ c/PCU) or that are short ($t_{\text{dur}} \lesssim 20$ s) E_b and t_{dur} do not correlate with $\langle F_{\text{pers}} \rangle$ ($\rho = -0.04$ in both cases), for energetic and long bursts a positive correlation is visible, that at least for E_b appears to be significant ($\rho = 0.46$ and 0.23 , respectively).

In other words, when looking at how the burst properties are influenced by the persistent emission, there is a dichotomy in behaviour between the mode-0 type II bursts, which have large fluences and long durations, and appear in the upper half of the plots, and mode-2 bursts, characterized by small fluences and short durations, appearing in the bottom half. Mode-1 bursts can clearly be found both in the lower half of the plots of Fig. 9 (low fluence and short duration) and in the upper half (large fluence and long duration). These are, respectively, the short bursts initiating the mode 1 sequence, and the long one that concludes it. These two groups inhabit the same regions of the plots as the mode-2 and -0 bursts, respectively.

The same threshold in fluence seems to determine the presence of a hump after a burst. Fig. 10 shows that, independent of burst mode, above a critical $E_b \sim 2 \times 10^4$ c/PCU, the burst fluence correlates with the ‘net’ (i.e. above $F_{\text{pers}}^{\text{min}}$) hump fluence E_{hump} . Again, bursts above this threshold are not only the mode 0, but also the resembling mode 1 that end a sequence of bursts and precede a hump.

4.3 Type I bursts in the mixed (hard) state

Various methods help identify the type I bursts in the sample. Their profiles in the light curves differ for a number of features from those of type II bursts. The type-I-burst peak fluxes are smaller than those of most type II bursts (type I bursts in the RB reach at most one-third of the Eddington luminosity; B13). Also, all type II bursts show multiple peaks in their decays, while type I bursts generally have smooth decays (but see B14). Finally, type I bursts have generally longer durations, causing the fast-recurring type II bursts to overlap with their exponential decays. Finding candidate type I bursts is therefore relatively straightforward.

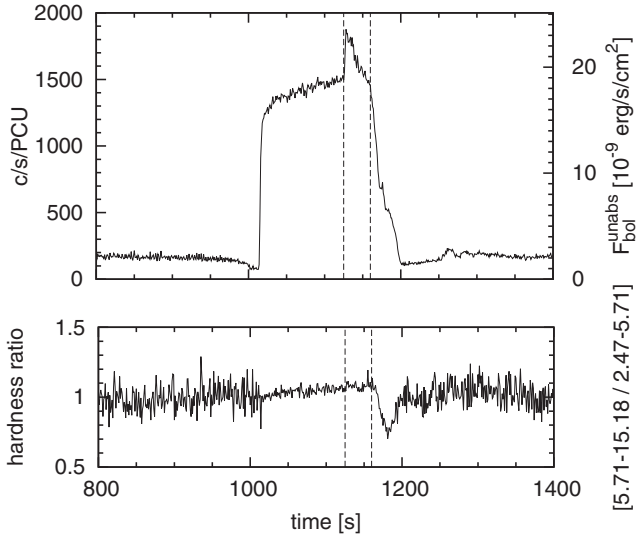


Figure 11. Light curve and hardness ratio of ObsID 50420-01-09-00R, featuring a type I burst taking place during a mode-0 type II burst. The vertical lines indicate the approximate start and end time of the burst. The net peak flux to persistent flux ratio $\beta \lesssim 0.2$, hiding the hardening of the flux during the type I burst below the detection level (Linares, Chakrabarty & van der Klis 2011; B13).

None the less, a secure identification of type I bursts should come from measurements of α or from the detection of cooling in their time-resolved spectra. However, the first method is only applicable in a state where *either* type I or II bursts are emitted. In a mixed state, where type II bursts recur faster than the type I bursts, one cannot rely on their α_{prev} values to discriminate between them. The second method, the detection of cooling, is only a sufficient, and not necessary condition for the type I burst identification. Observing spectral cooling is generally only possible for bright type I bursts ($F_{\text{peak}} \gtrsim 0.7F_{\text{pers}}$; Linares et al. 2011). B13 also showed that some RB bursts which lack evidence for cooling are to be identified as type I, due to their large α values and their occurrence in the brightest phases of the soft state.

To determine the presence of cooling, we measured hardness ratios as the flux ratios in the 5.1–7.6 keV and 2.3–5.1 keV bands. 26 candidate bursts show secure evidence of cooling, and we can therefore confirm they are type I even without being able to measure their α values.

Additionally, we found three bursts taking place ‘on top’ of a mode-0 type II bursts (see Fig. 11). For these bursts $F_{\text{peak}} \lesssim 0.2F_{\text{pers}}$, meaning the lack of cooling in their spectra cannot rule out their type I nature. Given their distinctive shape (fast rise and exponential decay), these three bursts are unlikely to be a sudden spike of the type II bursts, which tend to show nearly flat plateaus (see Section 2.2). Therefore, we believe they are type I bursts as well.

Summarizing, we found a total of 29 type I bursts occurring in an observation where also type II bursts appeared, out of a total of 123. Note that 17 candidate type I bursts could not be confirmed.

As shown in Fig. 12, the type I bursts in the hard state are significantly different from those in the soft state. Most remarkably, the durations are much shorter, with $t_{\text{dur}} \lesssim 40$ s, as are the peaks, that lack the 6–8 s plateau displayed by type I bursts in the soft state (B13).

Out of 29 type I bursts identified in the hard state, six took place around mode-0 type II bursts, 12 during mode 1, and 11 during mode 2. 10 out of 12 type I bursts found during mode-1 activity occur

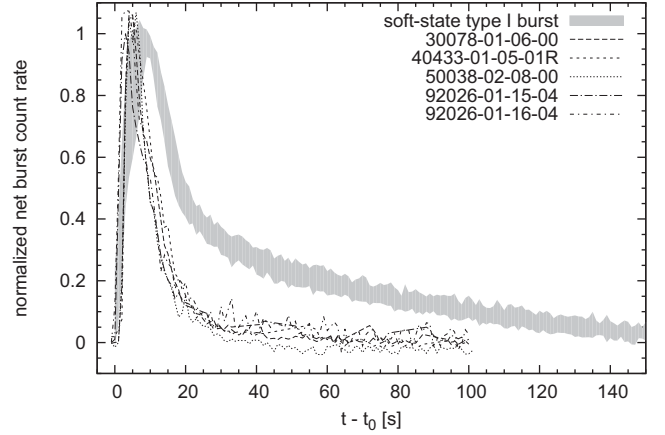


Figure 12. Light curves of five type I bursts in the hard state plotted against the average profile of the 22 single-peaked type I bursts featuring the longest and brightest decays (see B14), all of which are instead observed in the soft state. The net bursts counts have been normalized so that the average flux during the burst peak (which is defined as the interval during which the flux is above 90 per cent of the burst peak flux) is 1. The vertical extent of the shaded region indicates the standard deviation of the soft-state sample. The hard-state type I bursts were randomly chosen among those taking place on top of a stable persistent emission, i.e. outside humps, and showing no overlapping type II bursts during the first 40 s of the type I burst.

during the intervals of enhanced persistent emission (‘humps’) that are observed between two more tightly packed sequences of type II bursts (see Fig. 13, top). Only two type I bursts are instead observed ‘inside’ a sequence of mode-1 type II bursts. No such preferential location is observed for the 11 type I bursts occurring during the mode-2 phase, when the persistent emission count rate and the recurrence time of the type I bursts are roughly constant. However, it must be noted that one such type I burst seems to briefly (< 50 s) affect the type II emission (see Fig. 13, bottom), which is otherwise stable in this observation, as is common in mode 2.

For mode-1 type II bursts, one can calculate the chance of random coincidence of a hump and a type I burst. We examined all the mode-1-burst sequences during the outburst plotted in Fig. 1, and summed the integrated fluence from the beginning of each burst in a sequence until the last, longer one. We divided this integrated energy by the fluence emitted during the following hump. Over the course of the outburst, this ratio decreases from 13.5 to 2.7. In order to reach a conservative estimate, we take the latter as the ratio of the amount of mass accreted during a mode-1-burst sequence to that accreted during a hump. This means that, for each individual burst, the probability of random occurrence of a burst on a hump is $p_{\text{single}} = 0.27$. An estimate of the probability that 10 out of 12 type I bursts randomly take place on a hump rather than overlap with mode-1 bursts is thus given by the binomial distribution as $p_{10/12} = 7.24 \times 10^{-5}$. Clearly, type I bursts have a statistically significant preference for occurring during breaks in the type II activity, rather than overlapping them.

B13 reported type I burst recurrence times in the soft state in the range 0.4–4 ks. As the RB enters the hard state, t_{rec} becomes difficult to measure, as it typically surpasses the duration of an observation. The numbers should therefore only be treated as upper limits.

None the less, we can establish average recurrence times of type I bursts across the different modes of type II bursting. There are six confidently identified type I bursts in 114 ks of observations of mode 0, 12 in 170 ks of mode 1 and 11 in 492 ks of mode 2. If one includes the dubious cases, the type I bursts are 13 in mode 0,

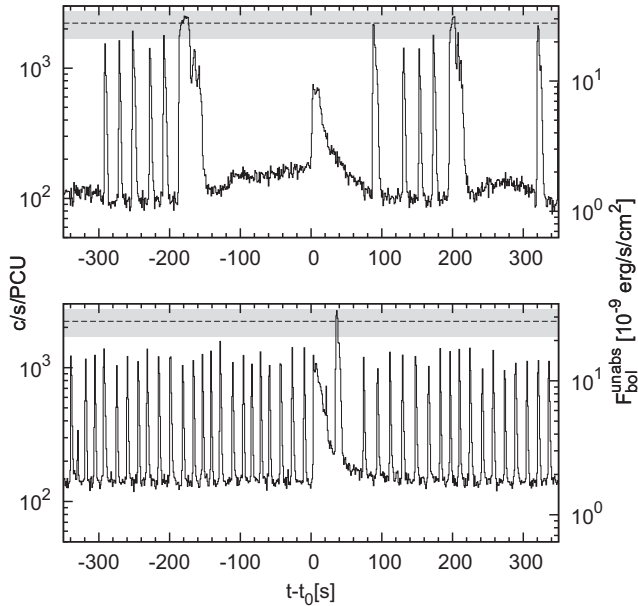


Figure 13. Two examples of type I bursts during the hard state, during mode 1 (top) and 2 (bottom) type II bursts, respectively. The x-axis shows time with respect to the type-I-burst start time t_0 . The y-axes are as in Fig. 1. The horizontal dashed line indicates the Eddington luminosity, with the grey-shaded area indicating the uncertainties on the distance and the spectral fit (see Section 3.1). Notice that the type I burst during the mode 1 phase takes place during the hiatus in type II bursts that follows a long one, while the persistent emission level rises in a hump shape. This is the case for 10 out of 12 type I burst during the mode 1 phase. Neither effect is observable as a type I burst takes place in the mode 2 phase (see Section 4.3). The type I burst during the mode 2 phase briefly affects the type II burst emission. This is only observed in 1 case out of 11.

21 in mode 1 and 12 in mode 2. This gives upper and lower limits, respectively, on the average recurrence times: $\langle t_{\text{rec}}^{\text{mode}0} \rangle \sim (8.3\text{--}18.1)$ ks, $\langle t_{\text{rec}}^{\text{mode}1} \rangle \sim (8.1\text{--}14.1)$ ks and $\langle t_{\text{rec}}^{\text{mode}2} \rangle \sim (41.0\text{--}44.7)$ ks. Thus, the type I burst recurrence time is roughly the same during mode 0 and mode 1.

We plot these recurrence times in Fig. 14 together with the type I burst recurrence times measured in the soft state, against the persistent flux F_{pers} (B13). The latter was taken to be a proxy of the mass accretion rate on the source, and the data show a correlation, with $t_{\text{rec}} \propto F_{\text{pers}}^{-0.95}$. The $\langle F_{\text{pers}} \rangle$ parameter we define in Section 3.2 only measures the emission taking place between type II bursts, but these should also accrete nuclear fuel on to the surface. Therefore, we plot the type I burst recurrence times across the three modes versus both $\langle F_{\text{pers}} \rangle$ and F_{tot} , which includes the burst fluence in the average.

As Fig. 14 shows, regardless of the proxy that is chosen for the mass accretion rate, the largest recurrence time for type I bursts is observed during mode-2 type II bursts. Interestingly, observations line up with the relation extrapolated from the soft state when employing $\langle F_{\text{pers}} \rangle$, while for F_{tot} there appears to be a scarcity of type I bursts in the hard state, across all modes.

5 OBSERVATIONAL SUMMARY

The large sample of data we have studied allows us to address fundamental questions over the type II bursts in the RB. In this section, we first summarize the overall properties of the sample, starting with those that were already previously known.

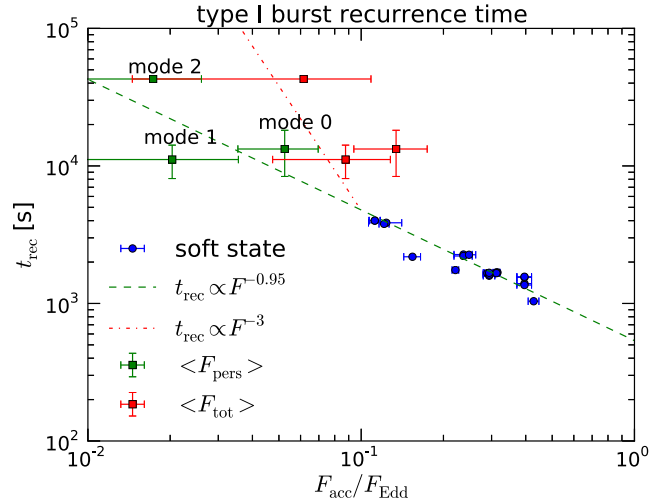


Figure 14. The recurrence time t_{rec} of type I bursts at different stages in the outburst. Blue points are soft-state measurements from B13, from which the fit is derived $t_{\text{rec}} \propto F_{\text{pers}}^{-0.95}$ (dashed line). Squares are averages for t_{rec} during mode-0, -1 and -2 phases, with the upper and lower limit derived using only securely identified type I bursts and including candidates, respectively (with a very small difference during mode 2). They are plotted against both the intratype II burst average flux $\langle F_{\text{pers}} \rangle$ and $\langle F_{\text{tot}} \rangle$, which includes the burst fluence in the average. The latter does not match the relation extrapolated from the soft state, but it is more compatible with a steeper $t_{\text{rec}} \propto F_{\text{pers}}^{-3}$ relation (dot-dashed line, see Section 6.4.)

(1) There are four patterns of type II bursts (e.g. Fig. 1).

(i) A (type II) burstless soft state that is visible when the persistent emission flux is above 10 per cent of the Eddington limit. This occurs mostly at the beginning of outbursts.

(ii) During the outburst decay, the first type II bursts to appear are of so-called mode 0 (Guerrero et al. 1999). They have the longest durations and recurrence times, and the largest fluences. The flat tops often observed in long mode-0 bursts are often sub-Eddington. Indeed, the flatness of the bursts has before been noticed to be a property of long bursts (Tan et al. 1991), regardless of their luminosity.

(iii) The mode-1 burst pattern follows, with sequences of frequent short bursts ending with a longer and brighter one that is similar in appearance to the shortest mode-0 bursts.

(iv) Finally, the mode-2 pattern appears, consisting of short bursts like the short ones in mode 1 (but not interrupted by larger bursts followed by longer recurrence times).

This is only a general rule and exceptions exist. For instance, the RB sometimes briefly switches back to the previous mode, and even back into the soft state. Mode-0 and -1 bursts can last for up to $\sim 5\text{--}6$ d, while mode-2 bursts persist for up to 24 d.

(2) The persistent emission decreases monotonically as the RB progresses from mode-0 to mode-1 to mode-2 bursts (Fig. 4). No type II bursts are observed on top of undetectable persistent emission.

(3) All bursts roughly follow a relaxation oscillator relation (Fig. 8, middle), meaning that the fluence in a burst determines the waiting time to the next burst.

(4) 95 per cent of the bursts show α values below 1.5, one order of magnitude below the minimum value that is possible for full thermonuclear burning. The distribution peaks at 0.2, meaning that five times more fluence is liberated in the bursts than in the persistent emission. This underlines the nature of type II bursts as accretion processes.

(5) We calculated the probability of random occurrence of the observed fraction of type I bursts on a hump to be $p_{10/12} = 7.24 \times 10^{-5}$. Clearly, type I bursts during mode 1 have a statistically significant preference for occurring during breaks in the type II activity, rather than overlapping them (see Fig. 13). This preference was first noticed in SAS-3 data by Ulmer et al. (1977), although it was Hoffman et al. (1978) who first proposed that the bursts on the humps and those surrounding them were type I and II, respectively. They also noticed that these bursts were ‘anomalous’ with respect to the type I bursts taking place during what we call mode 2, in that they had smaller peak fluxes and sometimes lacked spectral softening during burst decay. Likewise, we could confirm the presence of spectral softening in 11 out of 12 candidate type I bursts during mode 2, but only in 12 out of 21 during mode 1.

New findings in RB type II bursts are as follows.

(6) The range of minima in the persistent emission between bursts $F_{\text{pers}}^{\text{min}}$ is between 1 and 2.5 per cent of the Eddington luminosity. The distribution of the actual average persistent fluxes (i.e. taking the humps into account) (F_{pers}) extends to only slightly larger values, because the general sample is overwhelmingly dominated by the short mode-1 and mode-2 bursts, without humps in between. Taking into account the burst fluence as well, the RB is on average accreting at up to $\simeq 0.17L_{\text{Edd}}$ (Fig. 3).

(7) The persistent flux does not generally seem to correlate with the burst properties (Fig. 9). Each burst mode presents a large dispersion in the range of observed persistent fluxes (Fig. 4), making the latter a poor predictor of the burst mode.

(8) The most energetic type II bursts reach the Eddington limit ($F_{\text{Edd}} = 2.8 \times 10^{-8} \text{ erg cm}^{-2} \text{ s}^{-1}$; Fig. 5, top-left). 1 per cent of the bursts are super-Eddington. However, since the maximum $F_{\text{peak}}^{\text{max}} = 3.0 \times 10^{-8} \text{ erg cm}^{-2} \text{ s}^{-1}$, even a slight decrease in the H abundance or moderate beaming are enough to bring every single burst within the uncertainty on L_{Edd} (Section 3.1). Bursts reaching the Eddington limit are not accompanied by evidence for photospheric radius expansion (PRE) in the time-resolved spectra. Generally speaking, the peak flux shows no correlation with the waiting time or the persistent flux properties, and the distribution of peak fluxes is relatively narrow. Even the only visible correlation, the one with the burst fluence (Fig. 7), shows a large spread. This suggests that the speed at which energy is released does not depend on the total amount of energy available for a burst, nor on the global mass accretion rate.

(9) There is a clear dichotomy between mode-0 and mode-2 bursts. The former appear to feed back into the persistent emission, which rises in between them, while the latter do not seem to affect it. This is also reflected in the fact that only for mode 0 bursts there appear to be correlations between some properties of the bursts and of the persistent emission (Figs 8 and 9). Mode-1 bursts clearly are an intermediate state of the instability, reproducing both behaviours.

(10) Long bursts – meaning both mode-0 bursts and the mode-1 bursts that ‘close’ a sequence of bursts – are followed by humps, i.e. burst-free enhanced persistent emission. This is partially contrary to what was previously believed, that the persistent emission ‘dips’ between mode-0 bursts (Marshall et al. 1979; Kunieda et al. 1984; Stella et al. 1988; Lubin et al. 1992; Lewin et al. 1993; Guerriero et al. 1999), despite the fact that there is no evidence for enhanced absorption in the spectra (Stella et al. 1988; Lubin et al. 1993). However, looking at periods when the RB switches between these modes of emission, we clearly show that such ‘dips’ are actually at the same minimum level observed during a sequence of mode-1 bursts (Fig. 2). Since the persistent emission level is stable inside

a mode-1 sequence, and no increase in the column density N_{H} is observed in the spectra of the ‘dips’ (see Appendix B), we argue that in both cases the emission following a long burst is enhanced, to decay again in the time running to the next burst.

(11) The recurrence time distribution of type II bursts is strongly peaked at $\Delta t = 15\text{--}18$ s, and drops abruptly below this value, while showing a smoother decrease to larger recurrence times (Fig. 5). Bursts with shorter recurrence times are found (as short as 2 s) but they are a much smaller fraction of the sample, despite the fact that for a shorter Δt more bursts should be produced. This implies that a minimum time exists for the instability to develop, and that it is difficult for the RB to produce type II bursts more quickly than that.

(12) We found 61 bursts with durations shorter than 1 s, and as short as 130 ms (Fig. 6, top), one order of magnitude smaller than the shortest bursts so far reported for type II bursts (2 s in EXOSAT data; Lubin et al. 1991). This puts a constraint on theoretical models for this instability, that appears to cover four orders of magnitude in duration, up to the record observed $t_{\text{dur}} = 1100$ s.

(13) The sub-s duration bursts have α values between 20 and 200, thus overlapping with the α range of type I burst. Precursor events of sub-s durations have been observed before, but they are always followed by long type I bursts (in’t Zand, Keek & Cavecchi 2014). Therefore, the sub-s bursts are of type II.

(14) The relaxation-oscillator behaviour is more accurately predicted by the burst duration than the fluence (Fig. 8, bottom).

6 DISCUSSION

Having laid out all observational features of the type II bursts of the RB, we now discuss the physical implications of these. We leave the discussion of the instability models for type II bursts to the next section.

6.1 Accretion versus ejection

Two observables might suggest the possibility of mass ejection in the RB. One comes from the type I burst behaviour, which we discuss in Section 6.4. The second finding suggesting that mass could be ejected during type II bursts is that their peak flux never, for any persistent flux or burst fluence, surpasses a certain value which, within a factor of 2, is equal to the expected Eddington limit for an NS at the distance of the hosting globular cluster, with $X = 0.7$ and an isotropic radiation field (Figs 7–9). One might therefore wonder whether any surplus radiation power is transformed to the kinetic energy of an outflow enforced by radiation pressure.

There is, however, no spectral evidence for expansion of the emitting region. Thus, the picture arises that when the Eddington luminosity is reached, the accretion is temporarily halted, interrupting the release of gravitational energy. This in turn lowers the luminosity so that accretion can ensue again, rising back to the Eddington limit, and so on. The radiation pressure may momentarily cut off the fuel line for the radiation (the accretion flow), but not result in isotropic expansion. As a consequence of this, all energy is liberated through radiation, and there are no kinetic losses. This is in contrast to the type I bursts, where reaching the Eddington luminosity does not affect the energy release from the layer that has been heated by the burning, and the photosphere expands. Instead, once a type II burst flux reaches the Eddington luminosity, a larger fluence E_{b} can only be liberated by means of an increased duration, which makes for a tight relation between burst duration and fluence (Fig. 7, bottom).

6.2 Two kinds of type II bursts and three kind of modes

The data point to two kinds of type II bursts: long, often luminous ones and short ones. Long bursts, predominantly mode 0, occur at relatively larger mean accretion rates, while shorter ones abound at lower rates, during mode 2. They mix in mode 1. Long bursts induce humps and adhere more tightly to a relaxation oscillator behaviour, while the short ones are not followed by humps and show a larger scatter around the relaxation oscillator relation.

The evidence for this is provided in Fig. 9. At large $\langle F_{\text{pers}} \rangle$ one observes both long and energetic bursts, that become longer and stronger at larger persistent fluxes, and short and weak ones, displaying an opposite trend (i.e. becoming shorter and weaker at larger $\langle F_{\text{pers}} \rangle$). The critical fluence separating these two opposite feedbacks is $E_b \approx 2 \times 10^{39} \text{ erg s}^{-1}$. This duality is reflected by the way in which the bursts affect the persistent emission back. While short, weak burst do not have a feedback on F_{pers} , the long and strong bursts that appear in mode 0 and at the end of a mode-1 sequence generate humps of enhanced persistent emission. Fig. 10 shows that the threshold for this behaviour is again at $E_b \approx 2 \times 10^{39} \text{ erg s}^{-1}$.

Another look at Fig. 7 shows that the threshold in fluence at which the bursts become Eddington limited is $E_b \sim 5 \times 10^{38} \text{ erg s}^{-1}$. Notice that some mode-2 type II bursts reach $F_{\text{peak}} = F_{\text{Edd}}$, but very quickly decay, and are not followed by humps.

Possibly then, a sustained period of Eddington-limited emission is necessary for a type II burst to be followed by a period of enhanced persistent emission. It would therefore make more sense to speak of ‘short’ and ‘long’ bursts, rather than the three modes that are mentioned in literature. What Fig. 10 also shows, however, is that there is a continuity in behaviour between the two, rather than a clear cut distinguishing two different behaviours among type II bursts.

6.3 The relaxation-oscillator behaviour

Our data confirm the existence of the well-known relaxation oscillator between the burst fluence E_b and the time to the next burst Δt^{next} (Fig. 8, middle). However, we also find a tighter correlation between the burst duration t_{dur} and Δt (Fig. 8, bottom). It is quite possible that the relaxation-oscillator relation is a by-product of this tighter correlation and of the aforementioned one between E_b and longer t_{dur} . This would mean that it is the time-scales, rather than the energetics, that connect the bursts and the persistent emission.

The burst properties seem to depend weakly on the average intraburst persistent flux (Fig. 9). Also, relatively small changes in the persistent flux are visible between modes. The variations in the burst properties are therefore much larger than those in the accompanying persistent emission. In other words, the variation in the global mass accretion rate that must be present between the beginning and the end of the hard state is not equally split between the bursts and the persistent emission, but almost entirely goes into the former.

6.4 Type I bursts as a probe of mass accretion by type II bursts

Our data of type I bursts provide a test of the hypothesis that type II bursts are an accretion phenomenon. They provide an independent constraint on the accretion rate by comparing type I recurrence times with $F_{\text{pers}}^{\text{min}}$, $\langle F_{\text{pers}} \rangle$ and $\langle F_{\text{tot}} \rangle$. Fig. 14 shows that the type I burst recurrence time in the hard state matches the extrapolated fit to the soft state if $\langle F_{\text{pers}} \rangle$ is taken as a proxy of the mass accretion rate, which traces the persistent emission only. Adding the burst fluence to yield $\langle F_{\text{tot}} \rangle$ gives instead too long recurrence times, even if

one includes bursts for which the type I identification is tentative. In other words, taking into account the mass that type II bursts should be accreting on the NS surface does not yield the predicted recurrence times. There are three possible explanations for the mismatch between t_{rec} and $\langle F_{\text{tot}} \rangle$.

First, the type II bursts could be ejection rather than accretion events. The disproportionate coincidence in mode 1 of type I bursts with humps during type II burst intermission would then be explained by having mass accrete on to the NS only during these intermissions and not during type II bursts. Ejection is possible in a strong propeller regime, where the disc is truncated by the magnetosphere at sufficiently large radii ($r_m > 2^{1/3} r_{\text{cor}}$; Lii et al. 2014). The mechanism is similar to the one highlighted by D’Angelo & Spruit (2010, 2012, see below) with matter piling up and accreting in burst-like cycles. In this case, accretion is accompanied by the launch of a well-collimated, magnetically dominated Poynting jet. However, the predicted burst durations and recurrence times fall in the ms to s range, and very large B and small mass accretion rates (well below 10 per cent of the Eddington rate) are necessary. But the strongest argument against this hypothesis is that, in a propeller regime, the luminosity should drastically decrease with respect to the accreting regime, because the potential energy that would otherwise be liberated during the fall on to the NS surface will not be available (D’Angelo et al. 2015). As the type II bursts reach luminosities up to the Eddington limit, we are inclined to reject ejection as a valid hypothesis.

Secondly, the type I bursting rate could respond not only to the instantaneous mass accretion rate, but also on the rate at which it itself varies (i.e. \dot{m}). Possibly, the sudden and short-lived increase in \dot{m} associated with a type II burst will not produce the same effect in the burning layers as if the same mass had been more slowly accreted. To the best of our knowledge, however, simulations of how the type I burst behaviour changes with accretion rate only include models in which \dot{m} is constant over long periods of time (e.g. Heger, Cumming & Woosley 2007). It would perhaps be interesting to see what these models predict in case of swift, large and short-lived changes in the accretion rate, but we cannot presently elaborate further on this hypothesis.

Thirdly, the shorter duration of type I bursts in the hard state indicates that, as the mass-accretion rate decreases, the RB approaches a pure-He burning regime. In this case, a steepening of the relation in Fig. 14 is expected. Theoretical models predict a steeper relation in a pure-He regime (Cumming & Bildsten 2000), compatible with the $t_{\text{rec}} \propto \dot{m}^{-3}$ measured in IGR J17480–2446 (Linares et al. 2012, see their fig. 11). We plot this empirical relation in Fig. 14, assuming pure-He burning takes place for bursts below 10 per cent of the Eddington limit, at the state transition. This way we can account for the recurrence times plotted against $\langle F_{\text{tot}} \rangle$ during mode 1 and 2, although type I bursts remain underabundant for mode 0.

This last hypothesis has the advantage that it also explains the observed change in the type I burst duration. As already mentioned, type I bursts in the hard state are shorter than those in the soft state, both in total duration (~ 20 s, versus ~ 100 s in the soft state) and in the duration of their peaks (see Fig. 12). This is also ascribable to changes in the fuel composition: as the mass accretion rate decreases, the recurrence time of type I bursts lengthens, leaving less H unburnt by the hot CNO process, which in turn reduces the burst duration due to the lack of unstable H burning via the slow rp-process (Fujimoto, Hanawa & Miyaji 1981). This means that in the hard state the RB is approaching a pure-He burst regime. We think this is the most likely explanation of the three.

7 MODELS FOR TYPE II BURSTS

Since the discovery of type II bursts in the Rapid Burster, an assortment of instability mechanisms have been proposed for their origin. Bursts have been variously attributed to an instability in the accretion flow (either in viscosity or temperature), instabilities around the innermost stable circular orbit (ISCO) or as a result of the interaction between the accretion disc and a stellar magnetic field (e.g. Spruit & Taam 1993; Kuijpers & Kuperus 1994). In their review article, Lewin et al. (1993) give an overview of the various strengths and weaknesses of the different models. We proceed to review these models again and test their predictions against our observations of the population.

7.1 Type II bursts: a magnetic phenomenon?

7.1.1 Theory of disc–magnetosphere interactions

A weakness of many models proposed to explain type II bursts is the apparent uniqueness of the RB, since most proposed instabilities should be widely applicable. In this respect, models based on magnetospheric instabilities are perhaps the most promising, since a strong magnetosphere introduces new characteristic length-scales to the system, and the distinctiveness of the RB behaviour could then be attributed to an unusual magnetic field geometry (such as alignment with the rotation axis, e.g. Kuijpers & Kuperus 1994), or unusual relationship between the physical properties that determine the magnetic regulation of accretion and the properties of the accretion flow itself (in particular the accretion rate at which the state transition occurs). On the other hand, since X-ray pulsations have never been detected in the RB, it is not clear that there is a strong magnetic field in the system (although by the argument above this could be due to a near alignment between the rotation and the magnetic axes). The BP does have an estimated magnetic field and measured spin period ($B \sim (2\text{--}6) \times 10^{10}$ G, $P = 467$ ms; Finger et al. 1996; Degenaar et al. 2014). The observation of type I X-ray bursts in the RB puts an upper limit of $B \sim 10^{10}$ G for the field (based on measured fields of known bursters; Patruno & Watts 2012), but such a field would still be strong enough to truncate the accretion disc and regulate the gas flow in the inner regions of the star at moderate accretion rates (e.g. Pringle & Rees 1972). Magnetospheric instability models (studied both analytically and via numerical simulations) have also received the most theoretical development in the last 20 years (since the Lewin et al. 1993 review), so we concentrate our discussion on those results and how they compare with observation.

Accretion on to stars with strong magnetic fields becomes regulated by the magnetic field once it reaches a certain distance from the star (the ‘magnetospheric’, or ‘Alfvén’ radius, r_m). At r_m , the disc is truncated by the magnetic field, and the gas is channelled along magnetic field lines to accrete on the star (Pringle & Rees 1972; Shakura & Sunyaev 1973). The magnetospheric radius is typically approximated as the point where the ram pressure of the infalling gas equals the magnetic pressure of the field (with some considerable uncertainty from the fact that both the disc and the star are rotating; e.g. Ghosh & Lamb 1979; Spruit & Taam 1993):

$$r_m \simeq 3.1 \times 10^8 \left(\frac{\dot{M}}{10^{16} \text{ g s}^{-1}} \right)^{2/7} \left(\frac{M}{1.4 M_\odot} \right)^{-1/2} \times \left(\frac{B_*}{10^{10} \text{ G}} \right)^{4/7} \left(\frac{R_*}{10^6 \text{ cm}} \right)^{12/7} \text{ cm}. \quad (1)$$

The location of the inner disc radius is considerably uncertain and can vary with the spin rate of the star (Spruit & Taam 1993). A factor ~ 2 uncertainty for r_m should generally be assumed.

Since in general the disc and the magnetic field do not rotate at the same rate, the coupling between the two will twist the magnetic field lines, creating a torque that allows for angular momentum exchange between the disc and the star. The sign of the torque will depend on the location of r_m relative to the *co-rotation radius*, the radius at which the star’s rotation frequency Ω_* matches the Keplerian frequency of the disc:

$$r_c \equiv \left(\frac{GM_*}{\Omega_*^2} \right)^{1/3}. \quad (2)$$

Accretion can only proceed easily when $r_m < r_c$, that is, for relatively high accretion rates, slow stellar spin rates, and low magnetic field strengths. When $r_m > r_c$, the stellar magnetic field presents a centrifugal barrier to accretion, and either expels the infalling gas in an outflow (the ‘propeller’ scenario; Illarionov & Sunyaev 1975) or keeps it confined in the inner disc outside r_c (the ‘trapped disc’ scenario; Sunyaev & Shakura 1977; Spruit & Taam 1993; D’Angelo & Spruit 2010).

7.1.2 Trapped discs

The trapped-disc picture forms the bases of the most developed model to explain type II bursts in the RB. In this scenario, when the accretion rate falls below a certain rate, r_m (equation 1) moves outside r_c , and gas is no longer able to accrete on to the star. As long as r_m remains close to r_c , the disc–magnetosphere interaction will not provide enough energy to unbind the gas from the disc and launch an outflow. Instead, the gas stays confined in the disc, gradually piling up as more gas is accreted from larger radii. This situation continues until enough gas has piled up to push against the magnetic field for r_m to move inside r_c . Here, the centrifugal barrier disappears and the accumulated gas can rapidly accrete until the reservoir of gas has been depleted and r_m again moves outside r_c . Observationally, the instability will manifest as short outbursts (as gas accretes freely through the disc and on to the star) contrasted with periods of non-accretion (as gas gradually accumulates) with a roughly stable luminosity generated by the interaction between the disc and the magnetic field.

This instability was described and studied analytically and numerically in Spruit & Taam (1993), D’Angelo & Spruit (2010) and D’Angelo & Spruit (2012), who investigated its general properties (duty cycle, frequency, outburst shape, etc.) as a function of the mean accretion rate and the details of the disc–field interaction. In D’Angelo & Spruit (2010) and D’Angelo & Spruit (2012), the disc–field interaction is characterized by two (uncertain) length-scales: Δr , the radial extent of the disc that is coupled to the magnetic field and Δr_2 , the range of r_m around r_c where the disc changes from being a trapped disc (outside r_c) and accreting freely (inside r_c). A key feature of this instability is that it produces bursts on a wide range of time-scales, which can generally be much longer than the dynamical time-scale of the inner disc, and plausibly match the burst time-scales seen in the RB.

In the trapped disc instability, the main driver of changes in burst shape and duration is a changing mean accretion rate into the inner disc. Roughly speaking, the recurrence time increases and the burst duration and fluence decrease as the mean accretion rate decreases. This is broadly seen in the RB: the longest bursts in mode 0 occur early in the outburst, and the time between mode-2 bursts increases

gradually as the overall luminosity declines. If this instability is responsible for the behaviour seen in the RB, the stochastic behaviour seen in the variation between individual bursts is mainly attributable to a variable accretion rate in the inner disc regions. This may be consistent with the X-ray spectral transition from a disc-dominated ('soft' or 'high') state to a power-law dominated ('intermediate' to 'low') state. In NS and black hole binaries, the spectral transition to a power-law spectrum is typically accompanied by large luminosity fluctuations on a range of time-scales, which are commonly interpreted as fluctuations in local mass accretion rate propagated through the accretion flow (e.g. Lyubarskii 1997). Since the instability requires an accumulated mass reservoir, these accretion rate fluctuations will manifest as a variation in the duration and frequency of bursts.

However, the simulations of Spruit & Taam (1993) and D'Angelo & Spruit (2010) do not show the characteristic 'relaxation-oscillator' behaviour seen in type II bursts in the RB, where the wait time between bursts scales with the fluence of the previous burst. This is because neither set of simulations properly accounted for viscosity in the large-scale disc, which sets the time-scale to refill the inner disc regions. Instead, the simulations supplied gas into the inner regions of the disc at a steady rate, which leads to a steady burst period for a given accretion rate. In a realistic disc, if the reservoir of gas is emptied before the outer disc can resupply it with gas, the build-up time will be longer than has been observed in simulations. This introduces a new time-scale into the problem: the viscous refilling time. If the accretion rate into the inner disc is unsteady, the time-scale between bursts will be variable, but will be at least as long as it takes for gas to flow into the inner disc. This may account for the recurrence time–fluence relationship seen in Fig. 8: the recurrence time has a minimum (the viscous inflow rate) but can be much longer (if the supply rate suddenly decreases). D'Angelo & Spruit (2012) indeed found that a steadily decreasing accretion rate (in a large disc) can induce chaotic accretion bursts from the trapped disc instability (fig. 10 of that paper). This hypothesis remains to be investigated further.

D'Angelo & Spruit (2012) identified two distinct instability regions for the trapped disc instability: 'RI' (long duration, low amplitude bursts), and 'RII' (shorter, smaller amplitude bursts). In 'RI' bursts, $\Delta r_2/r \lesssim 0.02$ (i.e. the disc makes abrupt transitions between the accreting and non-accreting states), and the bursts often have complex profiles and with strong contrasts between bursting and interburst luminosity. In contrast, the 'RII' bursts occur at larger values of Δr_2 , bursts are more sinusoidal in shape with higher luminosities, shorter periods and less contrast between burst and interburst luminosities. The complex burst profiles and characteristic outburst time-scales of the mode-0 bursts suggest the RI instability is more likely applicable for the Rapid Burster.

At high mean accretion rates, the 'RI' accretion bursts are longer, with burst profiles that frequently show quasi-periodic oscillations (see Fig. 15) at the tail of the outburst, similar to mode-0 bursts of the RB. A flat-topped burst is also sometimes seen, although typically with an initial spike of accretion, which is not seen in RB mode-0 bursts. As the mean accretion rate drops, the burst duration and fluence decreases, and the bursts become more widely separated in time, similar to evolution in the mode-2 bursts of the RB (see Fig. 1).

7.1.3 Application to the RB

In comparing the predictions of the trapped disc model to the RB bursts, we consider only the short burst (mode-2 and short mode-1

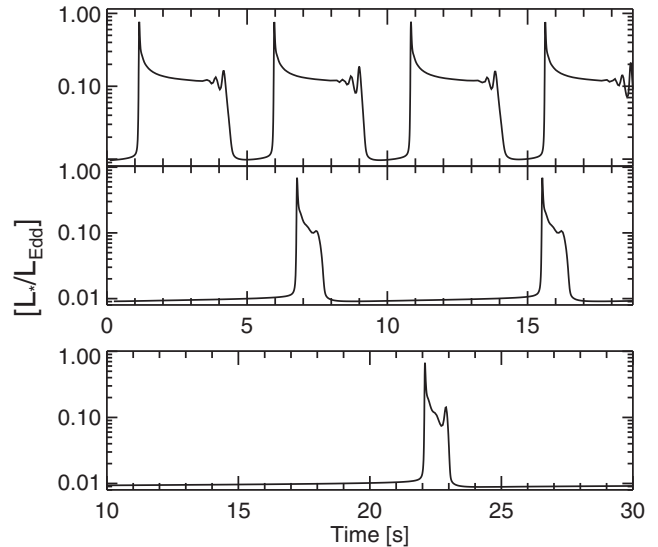


Figure 15. Bursts predicted by the trapped disc instability for an NS with $B = 10^{10}$ G and a spin period $P = 0.02$ s, for different mean accretion rates (see Section 7.1). From top to bottom, $\dot{M} = [0.03, 0.005, 0.002]\dot{M}_{\text{Edd}}$, with the burst fluence decreasing ($F = [7.8, 1.9, 1.8] \times 10^{38}$ erg) and recurrence time increasing as the mean accretion rate decreases. We plotted the properties of these simulated bursts against those of our sample in Fig. 7. The viscous response of the disc to the changing inner disc may create a delay in refilling the inner disc for larger bursts, reproducing the behaviour seen in the RB. Note that between bursts accretion in the inner disc is suppressed, and the disc luminosity is generated by the interaction between the disc and the magnetic field.

bursts). This is because the long mode-0 bursts have significantly different properties: they are often Eddington-limited bursts with a distinctive burst profile and persistent emission that shows a hump and (occasionally) type I bursts, suggesting significant accretion on to the star continues between bursts. We speculate that for mode-0 bursts, the trapped disc instability could appear in conjunction with a second physical process (perhaps related to the dramatic state change that marks the onset of type II bursts), but we do not consider this further.

Applying the trapped disc burst model to the RB is challenging, as its spin rate and magnetic field are unknown. However, if we assume (as this model would suggest) that the type II bursts begin when r_m moves just outside r_c , then the 'critical accretion rate' (that is, for the onset of bursts) is about $0.1 \dot{M}_{\text{Edd}}$. Equating r_m and r_c (equations 1 and 2) at this accretion rate leads to a degeneracy between B and P_* . We can set some bounds on these parameters from other evidence: the appearance of type I bursts suggests $B < 10^{10}$ G, while $P_* \gtrsim 0.0017$ s to make the RB compatible with the fastest rotating known NS. This leads to a range of $B \sim 6 \times 10^7 - 10^{10}$ G for spin periods $P \sim 2 - 80$ ms (with the fastest spin periods corresponding to the smallest magnetic fields). The smaller r_c , the nearer the disc will extend to the star, and the shorter the recurrence time will be between bursts, because the burst time-scale is generally set by the viscous diffusion time-scale, $t_{\text{visc}} \propto r_{\text{in}}^2/\nu$ in the disc's inner regions. For an α -disc viscosity, $\nu \sim \alpha(H/r)^2(GMr)^{1/2}$ (Shakura & Sunyaev 1973, where H is the scaleheight of the disc), so that for $\alpha \sim 0.1$, $(H/r) \sim 0.1$, $t_{\text{visc}} \sim 10 - 1000$ s at r_c for the range of possible spin periods. In D'Angelo & Spruit (2012), the strongest bursts occur on time-scales $0.1 - 10 t_{\text{visc}}$, which would correspond to 1–100 s if the RB is a rapid rotator and $100 - 10^4$ s if the spin frequency is lower. There is thus considerable degeneracy in the

model, but for a reasonable range of spin periods, magnetic fields and viscosities, it can reproduce the observable features of the RB.

In Fig. 15, we show bursts at three different accretion rates, choosing representative simulated parameters that reproduce the RB range of luminosity within the constraints on spin and magnetic field set above. We adopt $B = 10^{10}$ G, $P = 0.02$ s and a viscosity $\nu = 10^{-3}(GM\dot{M})^{-1}$, which gives strong bursts when the mean accretion rate decreases below ~ 10 per cent L_{Edd} . From top to bottom, the accretion rate decreases: $\dot{M} = [0.03, 0.005, 0.002]M_{\text{Edd}}$. The flux properties of the model agree quite well with the observed properties of the RB (see Fig. 7). The fluence in the bursts decrease from 7.8×10^{38} erg in the brightest burst to 1.8×10^{38} erg in the weaker bursts. In comparison, the RB shows bursts over a somewhat larger range of fluence, with 90 per cent of bursts between 0.13 and 1.8×10^{39} erg. The peak flux in the simulated bursts is nearly independent of accretion rate, which is also roughly consistent with the RB, where the peak luminosity of 90 per cent of the bursts spans a range of ~ 2 .

As discussed in Section 4.1, the persistent emission between bursts does not show obvious correlations with other burst properties, and varies by a factor ~ 2 for the majority of bursts. This is naturally accounted for by the trapped disc model, where between bursts accretion in the inner disc is suppressed, and the disc luminosity is generated by the interaction between the disc and the magnetic field, which adds angular momentum and energy to the disc. Since the location of the inner disc does not vary much between bursts, the luminosity also stays roughly constant, regardless of the fluence of the subsequent burst. As mentioned above, this does not account for the ‘humps’ and occasional type I bursts seen between long mode-0 bursts, since the distinctive nature of mode-0 bursts suggests additional physics beyond the theoretical picture outlined above.

The observed range of burst recurrence times and durations are less well accounted for in the model. As described above, all simulations of the instability assumed a constant accretion rate in to a small region of the inner disc, which does not properly account for the time it could take the disc to refill after an outburst. As a result, the recurrence time-scales linearly with accretion rate – the lower the mean accretion rate, the longer it takes to refill the reservoir and the weaker the subsequent burst. This is the opposite of what is apparently observed in the RB. However, if the accretion rate in the inner disc is strongly variable (as is postulated to explain rapid luminosity variability in the hard state; Lyubarskii 1997), the relationship between the mean accretion rate and burst fluence is less well defined. Simulations also show bursts with a smaller variation in burst durations (about a factor of 4, with durations between $\sim (2-8)$ s) than the RB, in which the majority of bursts (excluding mode 0, which as we argue above likely have an additional physical process governing their behaviour) last between 2–24 s, with a peak around 3 s.

In summary, the trapped disc instability can reasonably account for multiple properties of the RB short type II bursts for a variable accretion rate in the inner disc regions. Simulations can match observed burst fluences, maximum luminosities and persistent flux properties for reasonable (albeit poorly constrained) spin and magnetic field. The range of simulated burst durations and fluences are somewhat smaller (by a factor ~ 4 and ~ 2 , respectively) than is observed in the RB. Most significantly, the relaxation-oscillator behaviour is not reproduced, although as we argue above, this is at least in part because the response of the large-scale viscous disc to the burst instability has not been properly modelled. The finite viscosity in the disc will delay the refilling time once gas is depleted,

lengthening the time between bright bursts. The RB uniqueness may be explained by a special combination of magnetic field strength and stellar spin period (which together sets the accretion rate where the instability can manifest) and an alignment between the magnetic field and the spin axis.

7.2 Other magnetospheric instabilities

Several other mechanisms have been proposed to produce instabilities in the accretion flow that could explain the RB behaviour, but it is not clear that the time-scales on which they are expected to operate will match the RB. Both mechanisms outlined below rely on the ideal magnetohydrodynamic (MHD) properties of the accretion flow, i.e. that field lines are frozen in to the plasma and may not efficiently re-couple to the disc once the connection is severed (which is expected to happen rapidly due to differential rotation between the field and the disc). This can lead to either compression of the magnetic field by the disc moving inwards or unstable fingers of accretion on to the NS surface via interchange instabilities.

Kuijpers & Kuperus (1994) proposed that the perfectly conducting disc can be completely shielded from the magnetic field of the star, so that the disc will spiral inwards and pinch the dipolar magnetic field along the equator into a distorted ‘butterfly’ shape. This compression lasts until the matter touches the surface of the star, whereupon the gas penetrates through the field and accretes on to the star. This releases the pressure on the magnetic field, which rapidly re-expands and restarts the cycle. Some version of this scenario is seen in all magnetic accretion simulations (e.g. Hayashi, Shibata & Matsumoto 1996; Goodson, Winglee & Boehm 1997; Miller & Stone 1997; Romanova et al. 2009), which use ideal MHD and hence shield the disc from the magnetic field. However, due to the finite numerical diffusivity present in all simulations, the time-scale for the instability is typically a few dynamical time-scales, which is much shorter than the RB bursts ($\sim 50-1000$ dynamical times, depending on the spin of the star). Moreover, it is not at all clear theoretically that gas will have difficulty coupling to the magnetic field, as is required by this picture. Simulations of magnetorotational instability (MRI) in discs with stratified density profiles (e.g. Davis, Stone & Pessah 2010) show the disc field extends vertically out of the disc, which could form a low-density magnetized corona above the disc surface (e.g. Jiang, Stone & Davis 2014). This would provide an obvious site for reconnection, which could recouple the disc to the star and prevent strong compression of the magnetic field.

In this scenario, the burst should have a gradual rise (as the accretion disc spirals inwards towards the star) with a sudden spike when the gas finally hits the surface. This also seems inconsistent at least with the short bursts, which show low persistent emission between bursts, although it could perhaps explain the interburst humps seen between mode-0 bursts. In order to match the observed bursting time-scales, the original Kuijpers & Kuperus (1994) paper also posited a strong 10^{12} G field for the RB, which is inconsistent with the observation of type I X-ray bursts at relatively high luminosities.

An alternative scenario will develop when the field is not strong enough to efficiently disrupt the disc, allowing accretion to proceed via interchange (Rayleigh–Taylor) instabilities on to the star. In this picture, the RB magnetic field could be significantly weaker than assumed above (or the spin rate lower), so that the disc extends down to the star until the accretion rate drops to ~ 10 per cent L_{Edd} . At lower luminosities, the field will truncate the disc but not enough to enforce accretion on to the poles, and fingers of accretion will extend down to the stellar surface. This was studied in depth in the

in the 3D simulations of Kulkarni & Romanova (2008). However, as in the above scenario, the time-scale for the instability is typically the orbital time-scale of the inner disc edge, which will be smaller than the spin period of the star and thus likely considerably shorter than the observed burst time-scales unless the RB is a very slow rotator.

7.3 Thermal/viscous instability models

A number of models have also been proposed that do not rely on a role for the magnetic field. Lewin et al. (1993) have already reviewed them and explained their shortcomings; we will briefly discuss them in the light of our sample properties.

A class of models invokes thermal (Shakura & Sunyaev 1976) or viscous instabilities (Lightman & Eardley 1974) in the accretion disc to explain the luminosity fluctuations. Both instabilities arise in the inner portion of an α disc, where the radiation pressure dominates and electron scattering is the main source of opacity. Thermal instabilities are due to an inability to maintain a thermal balance, while viscous instabilities arise because the viscous stress becomes inversely proportional to the surface density, breaking up the inner disc in concentric rings as a result.

These analytical results however only established *local* criteria for instabilities to grow. They were first tested in a global, time-dependent simulation by Taam & Lin (1984), who confirmed the existence of unstable solutions. The produced bursts liberate about the right amount of energy ($10^{36} - 38$ erg), and the observed durations (0.1–1 s) and recurrence times (~ 10 s) at least overlap with the (however much broader) ranges observed in type II bursts. Also, the instability develops in a range of mass accretion rates ($(0.1 - 0.45) \times 10^{18}$ gs^{-1} , between 10 and 45 per cent L_{Edd}), above which the flow becomes stable again.

There are two main problems with this model. First, different time-scales and energetics can only be reproduced with variations of the global mass accretion rate. Although this problem is shared by the class of magnetospheric models discussed earlier, we should stress that at least in that case a much broader variety of burst properties is observed, closer to matching the ranges of fluences, durations and recurrence times that we have characterized in this study. Secondly, models relying on disc instabilities leave the uniqueness of the RB unaddressed, as they should apply to all accreting compact objects, even black hole binaries, and have indeed been put forward to explain the variability of sources like Cyg X-1.

7.4 GR models

An entirely different approach was taken by Walker (1992), who proposed that the RB be an exceptional source in hosting an NS with a radius smaller than the ISCO, surrounded by a massive accretion disc. The latter gives the very low viscosity the model requires. Also, the magnetic field must be weak enough not to disrupt the accretion flow. In this case, rather than having the magnetosphere act as a gate, radiation torques inside the ISCO lead to a sudden spike in the accretion rate, that repeats after the inner disc has been replenished on a viscous time-scale.

The predicted burst luminosities match those observed in type II bursts, and the bursts last between roughly 1 and 50 s. A very large disc would further be compatible with the large orbital period of the BP ($P_{\text{orb}} = 11.8$ d), while no orbit information is available for the RB. The model suffers from the same problem that afflicts all other models, namely the lack of a relaxation-oscillator behaviour. But its main shortcoming is that it cannot account for type II bursts

in the BP, which was only discovered three years after this model was proposed. Walker (1992) claim that the presence of a massive disc means that even relatively large magnetic fields (up to 10^{12} G) would not disrupt the Keplerian disc before it crosses the ISCO. Although estimates of the magnetic field strength in the BP are as low as $(2-6) \times 10^{10}$ G (Degenaar et al. 2014), there cannot be any doubt that magnetospheric accretion is happening in that source, because of the presence of pulsations at the spin frequency, both in the persistent emission and in the bursts. If GR effects were truly responsible for type II bursts in the RB, then another mechanism altogether would be at play in the BP.

8 CONCLUSIONS

Our population study has highlighted a number of new, important features of the type II bursts. The bursts are Eddington limited, which leaves little doubt as to their origin lying in accretion episodes. We have constrained the duration of these instabilities to cover the $10^{-1} - 10^3$ s range, and we have shown that a minimum recurrence time of order of 10 s seems necessary to develop a burst. We encourage dropping the old mode-0, -1 and -2 classification, adopting instead a simpler one between short and long bursts, which reflects the dichotomy these show in their interaction with the persistent emission.

We judge models based on thermal and viscous instabilities too general to explain the scarcity of sources displaying type II bursts, while models based on GR effects imply that a different phenomenon altogether is responsible for the BP bursts. Models based on the gating role of the magnetosphere can reproduce a number of properties in our sample, while at the same time requiring a fine tuning between the stellar spin, the magnetic field strength, the mass accretion rate and the alignment between the magnetic field and the spin axis, and thus account better for the uniqueness of the RB.

REFERENCES

- Bagnoli T., in't Zand J. J. M., Galloway D. K., Watts A. L., 2013, MNRAS, 431, 1947 (B13)
- Bagnoli T., in't Zand J. J. M., Patruno A., Watts A. L., 2014, MNRAS, 437, 2790 (B14)
- Cavecchi Y. et al., 2011, ApJ, 740, L8
- Cornelisse R. et al., 2003, A&A, 405, 1033
- Cumming A., Bildsten L., 2000, ApJ, 544, 453
- D'Angelo C. R., Spruit H. C., 2010, MNRAS, 406, 1208
- D'Angelo C. R., Spruit H. C., 2012, MNRAS, 420, 416
- D'Angelo C. R., Fridriksson J. K., Messenger C., Patruno A., 2015, MNRAS, in press
- Davis S. W., Stone J. M., Pessah M. E., 2010, ApJ, 713, 52
- Degenaar N., Miller J. M., Harrison F. A., Kennea J. A., Kouveliotou C., Younes G., 2014, ApJ, 796, L9
- Done C., Gierliński M., Kubota A., 2007, A&AR, 15, 1
- Finger M. H., Koh D. T., Nelson R. W., Prince T. A., Vaughan B. A., Wilson R. B., 1996, Nature, 381, 291
- Frogel J. A., Kuchinski L. E., Tiede G. P., 1995, AJ, 109, 1154
- Fujimoto M. Y., Hanawa T., Miyaji S., 1981, ApJ, 247, 267
- Galloway D. K., Muno M. P., Hartman J. M., Psaltis D., Chakrabarty D., 2008, ApJS, 179, 360
- Galloway D. K., Yao Y., Marshall H., Misanovic Z., Weinberg N., 2010, ApJ, 724, 417
- Ghosh P., Lamb F. K., 1979, ApJ, 232, 259
- Goodson A. P., Winglee R. M., Boehm K., 1997, ApJ, 489, 199
- Guerrero R. et al., 1999, MNRAS, 307, 179
- Hayashi M. R., Shibata K., Matsumoto R., 1996, ApJ, 468, L37
- Heger A., Cumming A., Woosley S. E., 2007, ApJ, 665, 1311

Hoffman J. A., Marshall H. L., Lewin W. H. G., 1978, *Nature*, 271, 630
 Illarionov A. F., Sunyaev R. A., 1975, *A&A*, 39, 185
 in't Zand J. J. M., Keek L., Cavecchi Y., 2014, *A&A*, 568, A69
 Jahoda K., Markwardt C. B., Radeva Y., Rots A. H., Stark M. J., Swank J. H., Strohmayer T. E., Zhang W., 2006, *ApJS*, 163, 401
 Jiang Y.-F., Stone J. M., Davis S. W., 2014, *ApJ*, 784, 169
 Keek L., Galloway D. K., in 't Zand J. J. M., Heger A., 2010, *ApJ*, 718, 292
 Kouveliotou C., van Paradijs J., Fishman G. J., Briggs M. S., Kommers J., Harmon B. A., Meegan C. A., Lewin W. H. G., 1996, *Nature*, 379, 799
 Kuijpers J., Kuperus M., 1994, *A&A*, 286, 491
 Kulkarni A. K., Romanova M. M., 2008, *MNRAS*, 386, 673
 Kunieda H. et al., 1984, *PASJ*, 36, 215
 Lewin W. H. G. et al., 1976, *ApJ*, 207, L95
 Lewin W. H. G., van Paradijs J., Taam R. E., 1993, *Space Sci. Rev.*, 62, 223
 Lightman A. P., Eardley D. M., 1974, *ApJ*, 187, L1
 Lii P. S., Romanova M. M., Ustyugova G. V., Koldoba A. V., Lovelace R. V. E., 2014, *MNRAS*, 441, 86
 Linares M., Chakrabarty D., van der Klis M., 2011, *ApJ*, 733, L17
 Linares M., Altamirano D., Chakrabarty D., Cumming A., Keek L., 2012, *ApJ*, 748, 82
 Lubin L. M., Lewin W. H. G., Tan J., van Paradijs J., van der Klis M., 1991, *MNRAS*, 252, 190
 Lubin L. M., Lewin W. H. G., Rutledge R. E., van Paradijs J., van der Klis M., Stella L., 1992, *MNRAS*, 258, 759
 Lubin L. M., Lewin W. H. G., van Paradijs J., van der Klis M., 1993, *MNRAS*, 261, 149
 Lyubarskii Y. E., 1997, *MNRAS*, 292, 679
 Mahasena P., Inoue H., Asai K., Dotani T., 2003, *PASJ*, 55, 827
 Marshall H. L., Hoffman J. A., Doty J., Lewin W. H. G., Ulmer M. P., 1979, *ApJ*, 227, 555
 Marshall H. L. et al., 2001, *AJ*, 122, 21
 Masetti N., 2002, *A&A*, 381, L45
 Masetti N. et al., 2000, *A&A*, 363, 188
 Miller K. A., Stone J. M., 1997, *ApJ*, 489, 890
 Morrison R., McCammon D., 1983, *ApJ*, 270, 119
 Patruno A., Watts A. L., 2012, preprint ([arXiv:e-prints](https://arxiv.org/abs/1205.3401))
 Pringle J. E., Rees M. J., 1972, *A&A*, 21, 1
 Raymond J. C., Smith B. W., 1977, *ApJS*, 35, 419
 Romanova M. M., Ustyugova G. V., Koldoba A. V., Lovelace R. V. E., 2009, *MNRAS*, 399, 1802
 Romanova M. M., Ustyugova G. V., Koldoba A. V., Lovelace R. V. E., 2012, *MNRAS*, 421, 63
 Rutledge R. E., Lubin L. M., Lewin W. H. G., Vaughan B., van Paradijs J., van der Klis M., 1995, *MNRAS*, 277, 523
 Shakura N. I., Sunyaev R. A., 1973, *A&A*, 24, 337
 Shakura N. I., Sunyaev R. A., 1976, *MNRAS*, 175, 613
 Shaposhnikov N., Jahoda K., Markwardt C., Swank J., Strohmayer T., 2012, *ApJ*, 757, 159
 Spruit H. C., Taam R. E., 1993, *ApJ*, 402, 593
 Stella L., Haberl F., Lewin W. H. G., Parmar A. N., van Paradijs J., White N. E., 1988, *ApJ*, 324, 379
 Strohmayer T., Bildsten L., 2006, in Lewin W. H. G., van der Klis M., eds, *New Views of Thermonuclear Bursts*. Cambridge Univ. Press, Cambridge, p. 113
 Suleimanov V., Poutanen J., Werner K., 2011, *A&A*, 527, A139
 Sunyaev R. A., Shakura N. I., 1977, *Sov. Astron. Lett.*, 3, 138
 Taam R. E., Lin D. N. C., 1984, *ApJ*, 287, 761
 Tan J., Lewin W. H. G., Lubin L. M., van Paradijs J., Penninx W., van der Klis M., Damen E., Stella L., 1991, *MNRAS*, 251, 1
 Titarchuk L., 1994, *ApJ*, 434, 570
 Titarchuk L., Lyubarskij Y., 1995, *ApJ*, 450, 876
 Ulmer M. P., Lewin W. H. G., Hoffman J. A., Doty J., Marshall H., 1977, *ApJ*, 214, L11
 Valenti E., Ferraro F. R., Origlia L., 2010, *MNRAS*, 402, 1729
 Valinia A., Marshall F. E., 1998, *ApJ*, 505, 134
 Walker M. A., 1992, *ApJ*, 385, 651
 Watts A. L., 2012, *ARA&A*, 50, 609

APPENDIX A: BURST SEARCH ALGORITHM

The thousands of type II bursts from the RB in the *RXTE* archive necessitate an automatic burst search algorithm for the identification process. We now proceed to explain the algorithm that we developed from trial and error. During the development, results were verified by visual inspection of the light curves.

The automatic procedure employs a light curve generated at 1 s resolution from all PCA 'STANDARD-1' data with the RB in the FOV (2.4 Msec), for all photon energies and for PCU2 which is the only PCU that is always on. Furthermore, the pointing and the elevation of the source above the Earth's horizon was tracked. From the pointing, the off-axis angle between the optical axis to the RB and 4U 1728-34 were calculated. Pointing and elevation information is available at 16 s resolution. For unsampled times, the pointing information was taken from the prior data point.

First, for each light-curve bin an estimate was made of the persistent emission underlying a potential burst at that bin, by determining the average of all flux values within 100 s prior to that bin, provided that the pointing is constant within 0.05 deg for at least the previous 5 s. If there was no reliable background from those data, the average flux was taken from the posterior 20 to 100 s interval. The background thus determined was subtracted from the flux of each bin. Secondly, a 'significance' was determined by taking the ratio to the Poisson error of that bin. If the significance was larger than 1, the bin was further investigated for the presence of a burst. Thirdly, the background-subtracted flux of subsequent bins after that bin were added to the signal and the accrued significance determined. This process was repeated for as long as the significance increased, allowing for it to decrease only once. When finished, an attempt was made to accrue signal going backward in time from the initial bin. Fourthly, the candidate burst was verified by checking that no other bursts previously determined (i.e. starting at earlier times) were in the new burst interval, that the total significance was at least 10, that the elevation was at least 2:5, that the pointing was constant during the burst and that there was at least one 'empty' bin between two consecutive bursts. A list of candidate bursts was thus composed. Since this allows for a more careful background determination from the original flux array by excluding the burst intervals and, fifth and last, the procedure was repeated. When it was impossible to determine the background, the burst was ignored.

All type I bursts from the RB show the typical fast-rise-exponential-decay (FRED) shape. Soft-state type I bursts have rise times (7.1 s) and durations (~ 100 s; B13), which are relatively long for type I bursts, and typical of the burning of H-rich fuel (Lewin et al. 1993). As we have shown in Section 4.3, hard-state type I bursts are typically shorter (~ 40 s). None the less, type II bursts of comparable durations cannot mimic the FRED shape, because multiple peaks appear in their decays (Tan et al. 1991). This allows identification of an RB type I burst even when its profile in the light curve overlaps with those of several fast-recurring type II bursts (as in Fig. 13, bottom).

As for type I bursts from 4U 1728-34, they show instead the much faster time-scales (rise time < 1 s, duration $\simeq 10$ s) that are typical of H-poor nuclear fuel (Galloway et al. 2010), and based only on this could be confused with short RB type II bursts. However, the bursts from 4U 1728-34 show a characteristic bimodal distribution of peak fluxes (9.2×10^{-8} erg cm $^{-2}$ s $^{-1}$ for the bursts showing photospheric radius expansion and 4.5×10^{-8} erg cm $^{-2}$ s $^{-1}$ for normal bursts; Galloway et al. 2008), which are much larger than observed in RB type II bursts. Still, when the PCA is pointed at the RB the peaks fluxes of the weakest 4U 1728-34 bursts can be similar to those of

the brightest RB type II bursts. Again, the multiple peaks in the decays reveal the nature of the latter.

Thus, a list of 8754 bursts was derived. 18 of these concern overlap between two kinds of bursts. The breakdown of three kinds of bursts is: type I bursts from the RB (123, 9 overlapping), type-I bursts from 4U 1728-34 (167, 9 overlapping) and type II bursts from the RB (8458, 18 overlapping). 22 bursts could not be definitely identified because of insufficient statistics. They are either type I from the Rapid Burster or type II. Otherwise, type-I bursts from 4U 1728-34 are easily recognizable because they are approximately two times brighter than the brightest type II bursts from the RB and last the shortest. The latter characteristic is necessary for identification because, when the PCA points at the RB and 4U 1728-34 is an off-axis angle of 0.5° , the collimator shadow cuts the measured peak flux in roughly two and is comparable to the brightest bursts of the RB. For the other two pointing configurations, identifying bursts from 4U 1728-34 is unambiguous. The difference between type I and II bursts from the RB is also manageable. Type I bursts are at least 20 s long, have a typical long tail (Bagnoli et al. 2013, 2014) and show no ringing, contrary to most type II bursts.

The start and end times of the bursts were determined by searching, starting from the bin with the highest flux, downward and upward, respectively, for the last times when the flux drops below 10 per cent of the peak flux. Notably, we identified a record duration for a mode-0 burst. Observation ID 92026-01-06-03 apparently starts off during a type II bursts which subsides only after 1100 s in a fashion typical for a mode-0 burst.

APPENDIX B: SPECTRAL ANALYSIS

In principle, one would like to perform a full time-resolved spectroscopic analysis of each type II burst to determine parameters such as peak flux (in $\text{erg cm}^{-2} \text{s}^{-1}$), burst fluence (in erg cm^{-2}), fluence of the persistent emission between bursts and α . However, given previously published spectral analyses of RB data (e.g. Marshall et al. 1979, 2001; Rutledge et al. 1995; Mahasena et al. 2003), there is merit in asking whether that is necessary. Spectral variability during and between type II bursts is presumably limited and the average energy per photon is probably nearly constant. In order to verify this and determine a conversion factor between PCA-detected photons and energy, we analysed a representative subset of the data. The subset was drawn from the ‘offset’ observations that are free from contamination by 4U 1728-34. 11 observations, identified by unique ObsIDs, were chosen representing typical as well as extreme behaviour of the RB. They are listed in Table B1.

The time resolution of the spectral analysis varied across the different observations and within observations is chosen to follow the variability in flux. In total, 374 spectra were extracted from these 11 observations, involving eight mode-0 bursts (including the longest one detected), 25 mode-1 bursts and 23 mode-2 bursts.

The spectral analysis involves the following generalities. Spectra were extracted from event-mode data with 64 spectral channels. All active PCUs were employed. The bandpass was limited to 2.5–20 keV which is where the PCA is well calibrated (Jahoda et al. 2006; Shaposhnikov et al. 2012) and contains most of the signal. A systematic error of 0.5 per cent per channel was included (following Shaposhnikov et al. 2012). All spectra were corrected for particle background and cosmic diffuse background as predicted through the PCABACKEST tool (version 3.8). The PCA response matrix was calculated with version 11.7.1 of tool PCARSP. This includes a correction for the collimator response which is always non-standard because the RB is always considerably off-axis in the selected ObsIDs. The collimator throughput for the RB was usually about 0.4. Spectral bins were combined to obtain at least 20 counts per bin to ensure applicability of the χ^2 statistic. All spectral modelling was carried out with XSPEC version 12.8.2. A constant cold interstellar absorption component was assumed to apply, equivalent to $N_{\text{H}} = 1.6 \times 10^{22} \text{ cm}^{-2}$ (Frogel, Kuchinski & Tiede 1995). The absorption model of Morrison & McCammon (1983) was followed.

A significant contribution may be expected from the Galactic Ridge. To determine this, off-axis observation ID 92026-01-04-00 was chosen which represents the observation with the lowest flux measured for the RB field. It was taken on 2006 June 9, 11 days before the onset of the outburst presented in Fig. 1. The background-subtracted data were modelled with the combination of a Raymond–Smith component (Raymond & Smith 1977) and a power law, following the prescription of Valinia & Marshall (1998) as also determined from PCA ridge data. The fit was satisfactory with $\chi^2_{\nu} = 1.79$ ($\nu = 20$). This constant spectral component was assumed to be present in all studied RB spectra.

We tested various models on the data: single component models (power law, Planck function, thermal bremsstrahlung, Comptonization) and models with combinations of two components. It was found that models with three free parameters were sufficient to describe all spectra. We chose the Comptonization model according to Titarchuk (1994) and Titarchuk & Lyubarskij (1995) as baseline since this is the simplest model fitting all data. Furthermore, we find that this model performs best to the highest quality spectrum (20093-01-07-01R whose spectrum contains 10^6 counts), with $\chi^2_{\nu} = 0.92$ for $\nu = 20$. As an example, for the same data $\chi^2_{\nu} = 11.3$ for a model consisting of a disc blackbody and a power law, and

Table B1. A representative subset of RB observations for spectral studies.

ObsID	Date of observation	Type of behaviour	Bolometric flux range ($10^{-8} \text{ erg cm}^{-2} \text{ s}^{-1}$)
20418-01-01-01R	1997 June 17	Bright soft state	1.2
20093-01-07-01R	1997 June 26	High soft state	1.3
20418-01-07-00	1997 July 10	Fainter soft state	0.26
30424-01-01-02R	1998 August 25	Mode 0, short bursts	0.1–1.7
30424-01-02-02R	1998 August 29	Mode 1, sequence of 5 bursts	0.1–2.5
30424-01-03-02R	1998 September 1	Mode 1, sequence of 20 bursts	0.1–2.8
30424-01-04-02R	1998 September 4	Mode 2, sequence of 22 bursts	0.1–0.8
30424-01-06-01R	1998 September 10	Mode-2, single burst in tail outburst	0.1–0.8
92026-01-06-00	2006 June 23	Mode 0, sequence of 5 short bursts (brightest fluxes from RB)	0.2–3.3
92026-01-06-03	2006 June 26	Mode 0, record-long burst (>1300 s)	0.15–0.8
92026-01-06-04	2006 June 27	Temporary return to soft state	0.45–0.55

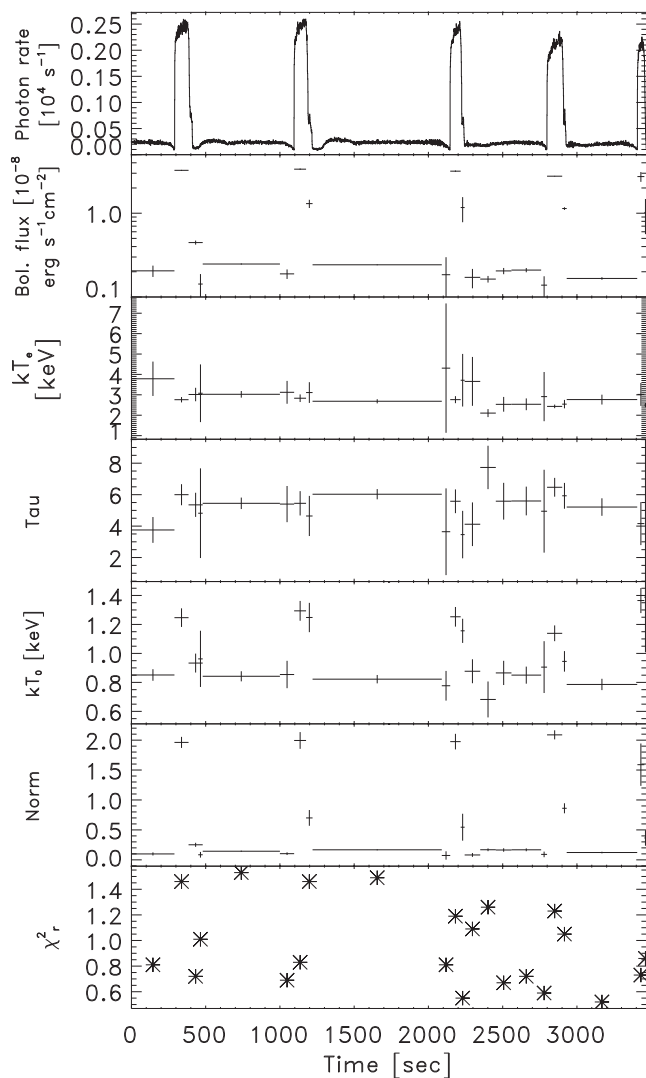


Figure B1. Time-resolved spectroscopy for ObsID 92026-01-06-00. The response is corrected for the off-axis position of the RB. The fitted model is the Comptonization model according to Titarchuk (1994).

6.88 for a cut-off power law. We note that it was necessary to complement the continuum model with a narrow line at about 6.5 keV, in the spectral region where the Fe-K resonance line resides (6.4–6.9 keV, depending on the ionization state of Fe). Possibly, it is related to instrumentally scattered emission from the bright source 4U 1728-34 just outside the FOV, or to an inadequate modelling of the Galactic Ridge at this location.

Fig. B1 shows an example of a time history for observation 92026-01-06-00 which shows a sequence of five bright and relatively short mode-0 bursts. What is clearly visible here, and that applies in general to all our spectral results, is that plasma temperature and optical depth show no significant variability, while photon seed temperature does. The plasma temperature varies in general between 2.5 and 3.5 keV while at the same time the plasma optical depth varies between 7 and 4, both typical 1σ errors of 1 in value. A more

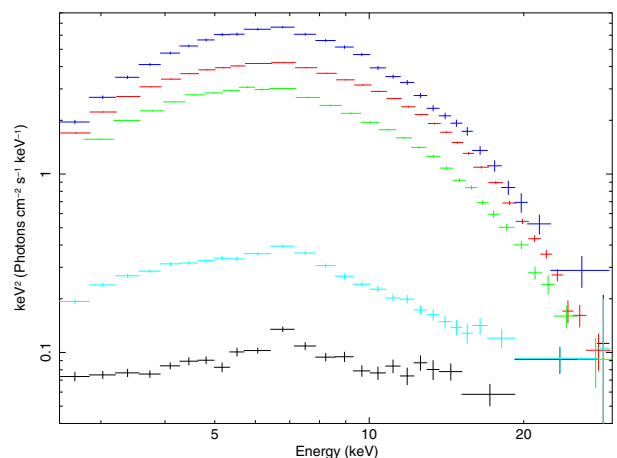


Figure B2. Unfolded 2.5–30 keV $\nu - f_\nu$ spectra for five widely different states of RB. From bottom to top: non-burst emission between slow mode-2 bursts (black curve, ObsID 30424-01-06-01R), non-burst emission in long intermission between mode-1 bursts (light blue; 30424-01-02-02R), peak of longest mode-0 burst ever measured (green; 92026-01-06-03), soft state prior to mode-0 (red; 20418-01-01-01R), peak of bright short mode-0 burst (dark blue; 30424-01-01-02R). The lowest spectrum shows the iron line clearly whose origin is undetermined.

detailed analysis of the spectral data is subject for a future paper. We here confine the analysis to inferring an average translation factor between photon fluxes and fluences and energy fluxes and fluences.

For the most accurately determined 112 spectral shapes, we find that a photon flux of $1 \text{ c s}^{-1} \text{ PCU}^{-1}$ for the whole band-pass translates on average to a 2.5–20 keV energy flux of $(1.02 \pm 0.02) \times 10^{-11} \text{ erg cm}^{-2} \text{ s}^{-1}$. All 112 conversion values are contained within 7 per cent from this average. Thus, the maximum systematic error by assuming a constant conversion factor is 7 per cent. Converting from 2.5–20 keV energy flux to unabsorbed bolometric flux involves a factor of 1.24 ± 0.07 . All 112 bolometric correction factors range between -7 per cent and $+2$ per cent from the mean. Therefore, the maximum systematic error in the bolometric correction factor is 7 per cent.

In Fig. B2, we show spectra of the five most diverse states of the RB. The conversion factor from $\text{c s}^{-1} \text{ PCU}^{-1}$ to unabsorbed bolometric $\text{erg cm}^{-2} \text{ s}^{-1}$ varies between 1.23×10^{-11} and 1.56×10^{-11} .

SUPPORTING INFORMATION

Additional Supporting Information may be found in the online version of this article:

(<http://mnras.oxfordjournals.org/lookup/suppl/doi:10.1093/mnras/stv330/-/DC1>).

Please note: Oxford University Press is not responsible for the content or functionality of any supporting materials supplied by the authors. Any queries (other than missing material) should be directed to the corresponding author for the paper.

This paper has been typeset from a $\text{T}_{\text{E}}\text{X}/\text{L}_{\text{A}}\text{T}_{\text{E}}\text{X}$ file prepared by the author.